Mathematics

http://www.aimspress.com/journal/Math

AIMS Mathematics, 11(8): 27018–27055.
DOI: 10.3934/math.20261083
Received: 07 June 2026
Revised: 31 July 2026
Accepted: 05 August 2026
Published: 27 August 2026

Research article

New discrete Ramos–Louzada exponential–type distribution with applications to biological and COVID-19 data

Ahood Abdalrahman Alazwari[1], Ayşe Metin Karakaş[2], Fatma Bulut[3], Eslam Hussam[4,5], Muhammad Ahsan-ul-Haq[6], Samirah Alzubaidi[7], Amani Alrumayh[8] and M. E. Sobh[9,*]

[1] Department of Mathematics, Faculty of Science, Al-Baha University, Al-Baha, Saudi Arabia
[2] Statistics department, Faculty of Arts and Sciences, Bitlis Eren University, Bitlis
[3] Mathematics department, Faculty of Arts and Sciences, Bitlis Eren University, Bitlis
[4] Department of Accounting, College of Business Administration in Hawtat Bani Tamim, Prince Sattam bin Abdulaziz University, Saudi Arabia
[5] Mathematics department, Faculty of Science, Capital University, Cairo, Egypt
[6] College of Statistical Sciences, University of the Punjab, Lahore, Pakistan
[7] Department of Mathematics, Al-Qunfudah University College, Umm Al-Qura University, Mecca, Saudi Arabia
[8] Department of Mathematics, College of Science, Northern Border University, Arar, Saudi Arabia
[9] Department of Mathematics, Faculty of Science, Mansoura University, Mansoura, Egypt

* **Correspondence:** Email: mohamedebrahim2014@mans.edu.eg; Tel: +20101710026.

Abstract: In this study, we introduced a novel discrete probability model, the discrete Ramos–Louzada exponential distribution, obtained by discretizing the survival function of its continuous counterpart. With a flexible two-parameter structure, the model captured diverse behaviors observed in count data. Core distributional properties, including the probability mass function, cumulative distribution function, survival function, hazard rate, and moment-generating function, were derived analytically. Log-concavity and an increasing hazard rate are established, supporting suitability for reliability and lifetime-type counts. Parameters were estimated using the maximum likelihood and Bayesian approaches, and finite-sample performance was evaluated through extensive simulation studies. Practical applicability was illustrated using European corn-borer larvae counts and daily COVID-19 mortality data from South Korea. Comparative goodness-of-fit results against established discrete models demonstrated superior performance, highlighting effectiveness.

Keywords: discrete distribution; Ramos–Louzada exponential distribution; survival discretization; parameter estimation; COVID-19 data

Mathematics Subject Classification: 62E15, 62F10, 62F15, 62N05

1. Introduction

In many scientific fields, such as ecology, epidemiology, insurance, and reliability engineering, empirical count and lifetime data often exhibit complex features, including overdispersion or underdispersion, skewness, and nonstandard tail behavior, which are not adequately captured by classical discrete models. Although the Poisson distribution is the most commonly used model for count data, its inherent equi-dispersion assumption substantially limits its applicability in practice. Similarly, continuous lifetime distributions such as the exponential or Weibull models are unsuitable when the observed failure times or event counts are intrinsically discrete. To address these challenges, a wide range of alternative discrete formulations has been proposed in the literature. In particular, the discretization of well-established continuous lifetime models has emerged as an effective strategy for constructing flexible and interpretable discrete distributions. By exploiting the survival function of a continuous baseline model, this approach preserves essential reliability characteristics while adapting the framework to integer-valued observations, thereby offering a principled and practical solution for modeling complex count data.

Discretization strategies preserve the essential properties of continuous-time models while enabling the analysis of count data. Several authors have contributed to the development of flexible discrete lifetime and count distributions.

A positive continuous random variable Y is said to follow the Ramos–Louzada exponential (RLE) distribution with shape parameters $\alpha > 0$ and $\beta \geq 2$, denoted by $Y \sim \mathrm{RLE}(\alpha,\beta)$, if its survival function (SF) is given by

$$\Psi(y;\alpha,\beta) = \left(1 + \frac{\alpha y}{\beta(\beta-1)}\right)\exp\left(-\frac{\alpha}{\beta}y\right), \quad y > 0. \tag{1.1}$$

Parameter α controls the overall decay rate of the distribution, whereas parameter β regulates the deviation from the classical exponential model, allowing for greater flexibility in modeling hazard rate behaviors. The RLE distribution, originally introduced by Aljohani et al. [4], extends the standard exponential distribution and exhibits appealing analytical and reliability properties, which make it a natural candidate for discretization in the context of count data modeling.

Exponentiated and extended discrete Lindley-type models were developed by El-Morshedy et al. [11], while the Burr–Hatke family was introduced in [12]. Eldeeb et al. [10] also proposed the discrete Ramos–Louzada distribution for asymmetric and over-dispersed data. Afify et al. [1] proposed a one-parameter discrete exponential model for COVID-19 data. Discretization-based extensions of classical lifetime models were further explored in [3,6]. Bayesian and classical inference frameworks were studied by Bernardo and Smith [7] and Carlin and Louis [9]. Discrete Gompertz-type models were introduced in [14, 15], while foundational discrete lifetime models include the discrete Weibull [16] and discrete Rayleigh distributions [19].

Despite the increasing number of discrete extensions of continuous lifetime models, there remains a persistent need for flexible and tractable discrete distributions capable of accurately modeling complex count data with skewness, heavy tails, and non-Poisson dispersion. Motivated by this need, introduce a novel two-parameter discrete probability model, the discrete Ramos–Louzada exponential (DRLE) distribution, constructed via the discretization of the continuous Ramos–Louzada exponential distribution via its survival function. While the continuous RLE model exhibits appealing structural and hazard rate properties, a principled discrete counterpart suitable for count data has not been formally developed.

Our primary objectives of this work are threefold. First, we formally define the DRLE distribution and derive closed-form expressions for its probability mass function, cumulative distribution function, survival function, hazard rate function, and associated reliability measures. Second, we establish key theoretical properties of the model, including log-concavity, unimodality, and monotonicity of the discrete hazard rate, which ensure interpretability and suitability for reliability-type count data. Third, we develop classical maximum likelihood and Bayesian inference procedures and evaluate their finite-sample performance through extensive Monte Carlo simulation studies. The empirical relevance of the proposed model is demonstrated through applications to real-world datasets from biology and epidemiology, including daily COVID-19 mortality counts, where comparative analyses confirm its superior or competitive goodness-of-fit relative to several well-known discrete distributions.

- Introducing the DRLE distribution as a flexible and parsimonious discrete model for skewed and overdispersed count data.
- Providing a comprehensive analytical study of the distribution, including closed-form expressions for core functions and rigorous characterization of shape and hazard rate properties.
- Developing and evaluating both maximum likelihood and Bayesian estimation frameworks, with small-sample behavior assessed via Monte Carlo simulations.
- Demonstrating the practical effectiveness of the DRLE model through real-data applications and systematic comparisons with established discrete alternatives.
- Establishing a foundational model that facilitates future extensions, including regression-based, zero-inflated, and hurdle-type DRLE models.

We note that the present applications involve marginal, cross-sectional count data rather than repairable-system failure processes; extending DRLE to dependent or multicomponent maintenance settings is discussed in the Future Research Directions.

The remainder of this paper is organized as follows: In Section 2, we introduce the DRLE distribution and derive its main statistical properties. In Section 3, we present the maximum likelihood and Bayesian estimation procedures. In Section 4, we report the results of the simulation study. In Section 5, we discuss real-data applications, and in Section 6, we conclude the paper with final remarks and directions for future research.

2. The DRLE distribution

In this section, we introduce the formal construction and main properties of the discrete Ramos–Louzada exponential (DRLE) distribution. The model is obtained by discretizing the continuous Ramos–Louzada exponential distribution through the survival–function approach.

2.1. Discrete Ramos–Louzada exponential random variable

Proposition 1. Let Y be a non–negative continuous random variable with survival function $\Psi(y; \alpha, \beta)$ defined in Eq (1.1). Define the discrete random variable

$$X = \lfloor Y \rfloor,$$

where $\lfloor \cdot \rfloor$ denotes the floor function. Then the probability mass function (PMF) of X is given by

$$p(x; \alpha, \beta) = \Psi(x; \alpha, \beta) - \Psi(x + 1; \alpha, \beta), \quad x = 0, 1, 2, \ldots \tag{2.1}$$

Substituting the survival function of the Ramos–Louzada exponential distribution into the above expression yields the PMF of the DRLE distribution as

$$p(x; \alpha, \beta) = \left[\left(1 + \frac{\alpha(x + 1)}{\beta(\beta - 1)}\right)\left(\frac{1 - \lambda}{\lambda}\right) - \frac{\alpha}{\lambda\beta(\beta - 1)}\right]\lambda^{x+1}, \quad x \in \mathbb{N}_0, \tag{2.2}$$

where $\lambda = \exp\left(-\frac{\alpha}{\beta}\right)$ and $\mathbb{N}_0 = \{0, 1, 2, \ldots\}$.

Definition 1. A discrete random variable X is said to follow a discrete Ramos–Louzada exponential distribution with parameters (α, β), denoted by $X \sim \text{DRLE}(\alpha, \beta)$, if its PMF is given by Eq (2.2).

Figure 1 illustrates the influence of the parameters α and β on the shape of the DRLE PMF, revealing a wide range of skewed and heavy-tailed behaviors suitable for modeling discrete lifetime and count data.

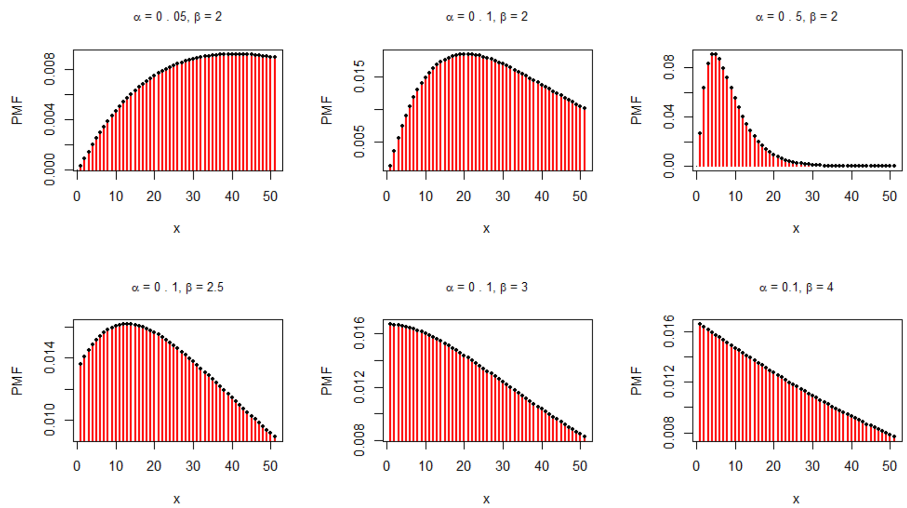

Figure 1. PMF curves of the DRLE distribution for different values of α and β.

Remark 1. The behavior of the DRLE PMF is characterized as follows:

(i) At $x = 0$,

$$p(0; \alpha, \beta) = -\frac{\alpha\lambda + \beta^2(\lambda - 1) - \beta\lambda + \beta}{\beta(\beta - 1)}.$$

(ii) As $\alpha \to 0$ (so that $\lambda \to 1$), $p(x; \alpha, \beta) \to 0$ for every fixed $x \in \mathbb{N}_0$.

Remark 2. The DRLE distribution contains the discrete Ramos–Louzada distribution of Eldeeb et al. [10] as a special case. Setting $\alpha = 1$ in Eq (1.1) gives

$$\Psi(y; 1, \beta) = \left(1 + \frac{y}{\beta(\beta - 1)}\right) e^{-y/\beta}.$$

This is exactly the DRL survival function with $\lambda = \beta$. Hence, DRLE(α=1,β) $\equiv$ DRL($\lambda = \beta$). DRLE also reduces to the Geometric($1 - e^{-\mu}$) distribution as $\beta \to \infty$ with $\alpha/\beta \to \mu$ fixed.

DRLE is not a reparameterization of the exponentiated discrete Lindley distribution [11], since EDL is constructed by exponentiating the CDF of the discrete Lindley distribution, a different mechanism from the DRLE construction. Unlike exponentiated discrete Lindley's exponent parameter, DRLE parameters α and β have a direct reliability interpretation, controlling the decay rate and the hazard shape, respectively.

DRLE is also mathematically distinct from discrete exponential-type models such as the discrete moment-exponential [1] and Poisson moment-exponential [2] distributions, which arise from discretizing or mixing a moment-exponential baseline and retain only a single shape parameter with a fixed hazard-rate structure. In contrast, DRLE's second parameter β provides an additional, independent degree of freedom that controls the curvature of the hazard rate without altering its monotonicity, enabling the model to accommodate a wider range of dispersion and zero-inflation behavior than these one-parameter exponential-type alternatives. This additional flexibility makes DRLE particularly suitable for count data exhibiting simultaneous over-dispersion and pronounced right-skewness or heavy tails, such as biological abundance counts and epidemic mortality counts, where one-parameter discrete exponential, Lindley or Ramos–Louzada models are structurally constrained to a single hazard shape and cannot adapt to both features at once.

2.2. *Distributional and reliability functions*

The cumulative distribution function (CDF) of the DRLE distribution is given by

$$F(x; \alpha, \beta) = 1 - \left(1 + \frac{\alpha(x + 1)}{\beta(\beta - 1)}\right) \lambda^{x+1}, \quad x \in \mathbb{N}_0, \tag{2.3}$$

and the corresponding survival function is

$$S(x; \alpha, \beta) = \left(1 + \frac{\alpha(x + 1)}{\beta(\beta - 1)}\right) \lambda^{x+1}, \quad x \in \mathbb{N}_0. \tag{2.4}$$

Remark 2. The behavior of the survival function is summarized as follows:

(i) At $x = 0$,

$$S(0; \alpha, \beta) = \lambda\left(1 + \frac{\alpha}{\beta(\beta - 1)}\right).$$

(ii) As $\alpha \to 0$, $S(x; \alpha, \beta) \to 1$ for every fixed $x \in \mathbb{N}_0$.

2.3. Hazard rate functions

An important reliability characteristic of discrete lifetime models is the hazard rate function (HRF), which describes the conditional probability of failure at time x. To avoid ambiguity, we explicitly adopt the following conventions: The survival function $S(x;\alpha,\beta)$ in Eq (2.4) represents $P(X > x)$, the HRF is defined as the conditional probability $h(x;\alpha,\beta) = p(x;\alpha,\beta)/P(X \geq x) = p(x;\alpha,\beta)/[1 - F(x-1;\alpha,\beta)]$, and the reversed hazard rate (RHRF) is defined as $r(x;\alpha,\beta) = p(x;\alpha,\beta)/F(x;\alpha,\beta)$. For the DRLE distribution, the HRF is given by

$$h(x;\alpha,\beta) = \frac{p(x;\alpha,\beta)}{1 - F(x-1;\alpha,\beta)} = \frac{\left(1 + \frac{\alpha(x+1)}{\beta(\beta-1)}\right)(1-\lambda) - \frac{\alpha}{\beta(\beta-1)}}{1 + \frac{\alpha x}{\beta(\beta-1)}}, \quad x \in \mathbb{N}_0. \tag{2.5}$$

The RHRF takes the form

$$r(x;\alpha,\beta) = \frac{p(x;\alpha,\beta)}{F(x;\alpha,\beta)} = \frac{\left[\left(1 + \frac{\alpha(x+1)}{\beta(\beta-1)}\right)(1-\lambda) - \frac{\alpha}{\beta(\beta-1)}\right]\lambda^x}{1 - \left(1 + \frac{\alpha(x+1)}{\beta(\beta-1)}\right)\lambda^{x+1}}, \quad x \in \mathbb{N}_0. \tag{2.6}$$

Remark 3. The behavior of the HRF is summarized as follows:

(i) At $x = 0$,

$$h(0;\alpha,\beta) = 1 - \lambda\left(1 + \frac{\alpha}{\beta(\beta-1)}\right).$$

(ii) As $\alpha \to 0$, $h(x;\alpha,\beta) \to 0$ for every fixed $x \in \mathbb{N}_0$.

Figure 2 demonstrates that the DRLE model is capable of capturing a variety of failure rate behaviors, highlighting its flexibility in discrete reliability analysis.

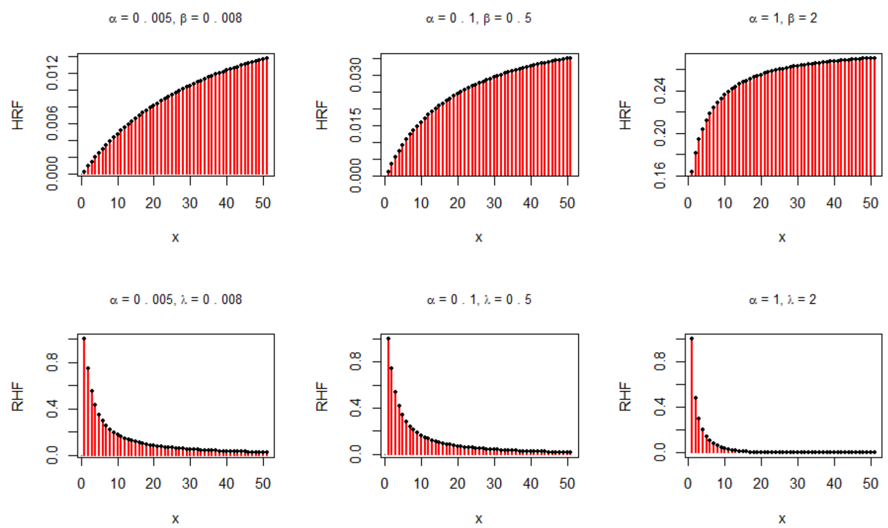

Figure 2. HRF and RHRF plots of the DRLE distribution for selected parameter values.

2.4. Shape properties

Lemma 2.1. For any $\alpha > 0$ and $\beta \geq 2$, the PMF of the DRLE distribution is log–concave.

Proof. A discrete distribution is log–concave if

$$p^2(x;\alpha,\beta) \geq p(x+1;\alpha,\beta)\, p(x-1;\alpha,\beta), \quad x \in \mathbb{N}_0.$$

Using the PMF in Eq (2.2), direct algebraic manipulation yields

$$p^2(x;\alpha,\beta) - p(x+1;\alpha,\beta)\, p(x-1;\alpha,\beta) = \frac{\alpha^2(\lambda-1)^2\lambda^{2x}}{(\beta-1)^2\beta^2},$$

which is strictly positive for all $\alpha > 0$ and $\beta \geq 2$. Hence, the PMF is log–concave. □

Lemma 2.2. Let $X \sim \text{DRLE}(\alpha,\beta)$. Then the mode θ_0 of X lies in the interval $\theta_0 \in [\theta_L, \theta_U]$, where

$$\theta_L = \frac{2\lambda}{1-\lambda} - \frac{\beta(\beta-1)}{\alpha}, \qquad \theta_U = \frac{1+\lambda}{1-\lambda} - \frac{\beta(\beta-1)}{\alpha},$$

and $\lambda = \exp(-\alpha/\beta)$. Moreover, if $\theta_U \leq 0$, then $\theta_0 = 0$.

Proof. Since the DRLE distribution is log-concave (Lemma 2.1), it is unimodal, so

$$p(x;\alpha,\beta) \geq p(x-1;\alpha,\beta) \;\text{ for } x \leq \theta_0, \qquad p(x;\alpha,\beta) \geq p(x+1;\alpha,\beta) \;\text{ for } x \geq \theta_0,$$

where θ_0 is the mode. From Eq (2.2),

$$p(x;\alpha,\beta) = \lambda^x \left[(1-\lambda) + \frac{\alpha}{\beta(\beta-1)}\Big((x+1)(1-\lambda) - 1\Big)\right].$$

Substituting into $p(x;\alpha,\beta) \geq p(x-1;\alpha,\beta)$ and dividing by $\lambda^{x-1}(1-\lambda) > 0$ gives, after simplification,

$$-(1-\lambda) + \frac{\alpha}{\beta(\beta-1)}\Big[(\lambda+1) - (1-\lambda)x\Big] \geq 0 \quad \Longrightarrow \quad x \leq \frac{\lambda+1}{1-\lambda} - \frac{\beta(\beta-1)}{\alpha} =: \theta_U.$$

Similarly, substituting into $p(x;\alpha,\beta) \geq p(x+1;\alpha,\beta)$ and dividing by $\lambda^x(1-\lambda) > 0$ gives

$$(1-\lambda) + \frac{\alpha}{\beta(\beta-1)}\Big[(1-\lambda)x - 2\lambda\Big] \geq 0 \quad \Longrightarrow \quad x \geq \frac{2\lambda}{1-\lambda} - \frac{\beta(\beta-1)}{\alpha} =: \theta_L.$$

Combining the two bounds, $\theta_0 \in [\theta_L, \theta_U]$, which proves the lemma. Since $X \in \mathbb{N}_0$, if $\theta_U \leq 0$ the mode collapses to $\theta_0 = 0$. □

Lemma 2.3. For any $\alpha > 0$ and $\beta \geq 2$, the hazard rate function of the DRLE distribution is strictly increasing in $x \in \mathbb{N}_0$.

Proof. Let $a = \dfrac{\alpha}{\beta(\beta-1)} > 0$ and $\lambda = e^{-\alpha/\beta} \in (0,1)$. Recall from Eq (2.5) that the hazard rate can be written as

$$h(x;\alpha,\beta) = (1-\lambda) - \frac{a\lambda}{1+ax}, \qquad x \in \mathbb{N}_0. \tag{2.7}$$

Taking the discrete forward difference of (2.7), we have

$$h(x+1;\alpha,\beta) - h(x;\alpha,\beta) = a\lambda\left[\frac{1}{1+ax} - \frac{1}{1+a(x+1)}\right] = \frac{a^2\lambda}{(1+ax)(1+a(x+1))}.$$

Since $\alpha > 0$ and $\beta \geq 2$ imply $a > 0$ and $\lambda \in (0,1)$, and since $1 + ax > 0$ and $1 + a(x+1) > 0$ for all $x \geq 0$, it follows that

$$h(x+1;\alpha,\beta) - h(x;\alpha,\beta) > 0, \qquad \forall\, x \in \mathbb{N}_0.$$

Hence $h(x;\alpha,\beta)$ is strictly increasing in x, for every $\alpha > 0$ and $\beta \geq 2$. □

3. Some statistical features

In this section, we present key distributional and reliability-related characteristics of the DRLE model, with emphasis on the moment generating function (MGF), characteristic function (CF), and raw moments. Throughout, let $X \sim \text{DRLE}(\alpha,\beta)$ with $\alpha > 0, \beta \geq 2$, and $\lambda = \exp(-\alpha/\beta)$.

3.1. Moment generating and characteristic functions

Proposition 2. Let $X \sim \text{DRLE}(\alpha,\beta)$. Then the moment generating function $M_X(t) = \mathbb{E}(e^{tX})$ is given by

$$M_X(t) = \frac{\dfrac{\alpha\lambda\,(e^t - 1)}{\beta(\beta-1)} + (\lambda - 1)\,(\lambda e^t - 1)}{(\lambda e^t - 1)^2}. \tag{3.1}$$

Proof. The result follows from the definition $M_X(t) = \sum_{x=0}^{\infty} e^{tx} f(x)$ and the closed-form PMF in (2.2). After substituting $f(x;\alpha,\beta)$, the resulting series can be summed using standard geometric-series identities, which yields (3.1). □

Corollary 1. The characteristic function $\varphi_X(t) = \mathbb{E}(e^{itX})$ is obtained by replacing e^t with e^{it} in (3.1), that is,

$$\varphi_X(t) = \frac{\dfrac{\alpha\lambda\left(e^{it} - 1\right)}{\beta(\beta-1)} + (\lambda - 1)\left(\lambda e^{it} - 1\right)}{(\lambda e^{it} - 1)^2}. \tag{3.2}$$

3.2. Raw moments

Proposition 3. Let $X \sim \text{DRLE}(\alpha,\beta)$. For any non–negative integer r, the rth raw moment $\mu_r' = \mathbb{E}(X^r)$ can be written as

$$\begin{aligned}\mu_r' &= \sum_{x=0}^{\infty} x^r f(x;\alpha,\beta) = \sum_{x=1}^{\infty} (x^r - (x-1)^r)\, S(x;\alpha,\beta) \\ &= \sum_{x=1}^{\infty} (x^r - (x-1)^r)\left(1 + \frac{\alpha(x+1)}{\beta(\beta-1)}\right)\lambda^{x+1}.\end{aligned} \tag{3.3}$$

Proof. The first equality follows from the definition of the raw moment. The second equality is obtained using the summation-by-parts identity for nonnegative integer-valued X,

$$\sum_{x=0}^{\infty} x^r f(x) = \sum_{x=1}^{\infty} (x^r - (x-1)^r) S(x),$$

together with the survival function $S(x; \alpha, \beta)$ in Eq (2.4). This yields (3.3). □

Corollary 2. Based on (3.3), the first four raw moments of the DRLE distribution are given by

$$\mu_1' = \frac{\lambda(\alpha + \beta(\beta + \lambda - \beta\lambda - 1))}{\beta(\beta-1)(\lambda-1)^2}, \tag{3.4}$$

$$\mu_2' = \frac{\lambda\left(\beta(\beta-1)(\lambda^2-1) - \alpha(3\lambda+1)\right)}{\beta(\beta-1)(\lambda-1)^3}, \tag{3.5}$$

$$\mu_3' = \frac{\lambda\left(\alpha\lambda(7\lambda+10) + \alpha - \beta(\beta-1)(\lambda-1)(\lambda(\lambda+4)+1)\right)}{\beta(\beta-1)(\lambda-1)^4}, \tag{3.6}$$

and

$$\mu_4' = \frac{\lambda\left(-\dfrac{\alpha\left(5\lambda(3\lambda^2+11\lambda+5)+1\right)}{\beta(\beta-1)} + \lambda^3(\lambda+10) - 10\lambda - 1\right)}{(\lambda-1)^5}. \tag{3.7}$$

3.3. Variance, skewness, and kurtosis

Using (3.4)–(3.7), the variance $V(X) = \mathrm{Var}(X)$, skewness (S.K), and kurtosis (K.U) of the DRLE distribution are obtained, respectively, as

$$V(X) = \frac{\lambda\left(-\alpha^2\lambda - \alpha\beta(\beta-1)(\lambda^2-1) + \beta^2(\beta-1)^2(\lambda-1)^2\right)}{\beta^2(\beta-1)^2(\lambda-1)^4}, \tag{3.8}$$

$$\text{S.K} = \frac{\begin{pmatrix} 2\alpha^3\lambda^2 - (\beta-1)^3\beta^3(\lambda-1)^3(\lambda+1) \\ + 3\alpha^2(\beta-1)\beta\lambda\left(\lambda^2-1\right) \\ + \alpha(\beta-1)^2\beta^2(\lambda-1)^2(\lambda(\lambda+4)+1) \end{pmatrix}}{\lambda^{\frac{1}{2}}\left[-\alpha^2\lambda - \alpha\beta(\beta-1)(\lambda^2-1) + \beta^2(\beta-1)^2(\lambda-1)^2\right]^{\frac{3}{2}}}, \tag{3.9}$$

and

$$\text{K.U} = \frac{\begin{pmatrix} -3\alpha^4\lambda^3 - 6\alpha^3\beta\lambda^2(\beta-1)(\lambda^2-1) \\ + \beta^4(\beta-1)^4(\lambda-1)^4(1+\lambda(\lambda+7)) \\ - \alpha\beta^3(\beta-1)^3(\lambda-1)^3(\lambda+1)(\lambda(\lambda+16)+1) \\ - 2\lambda\beta^2\alpha^2(\beta-1)^2(\lambda-1)^2(2+\lambda(2\lambda+11)) \end{pmatrix}}{\lambda\left[\beta^2(\beta-1)^2(\lambda-1)^2 - \alpha^2\lambda - \alpha(\beta-1)\beta(\lambda^2-1)\right]^2}. \tag{3.10}$$

Figures 3–6 display the empirical mean, variance, skewness, and kurtosis of the data, providing a concise summary of its central tendency, dispersion, asymmetry, and tail behavior.

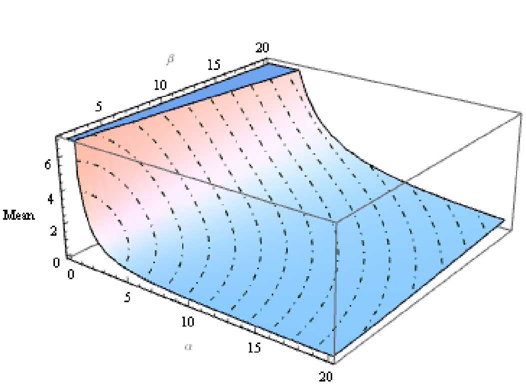

Figure 3. Mean.

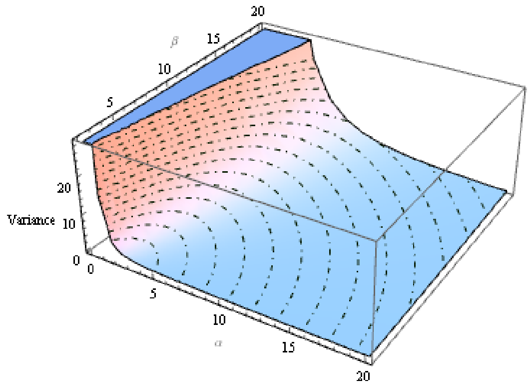

Figure 4. Variance.

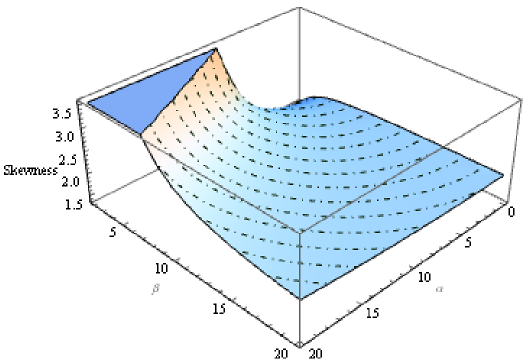

Figure 5. Skewness.

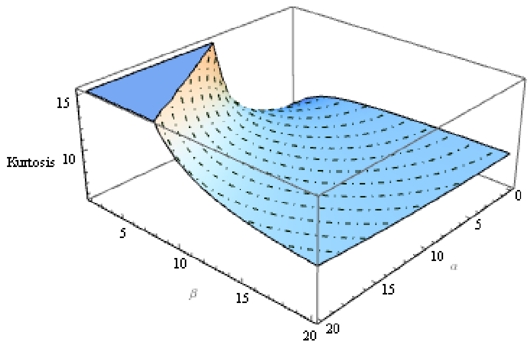

Figure 6. Kurtosis.

3.4. Dispersion and zero-modification measures

A standard dispersion summary for count models is the index of dispersion (IOD), defined as IOD $= V(X)/\mathbb{E}(X)$. For the DRLE model,

$$\text{IOD} = \frac{V(X)}{\mu_1'} = \frac{\alpha^2\lambda + \alpha\beta(\beta-1)(\lambda^2-1) - \beta^2(\beta-1)^2(\lambda-1)^2}{\beta(\beta-1)(\lambda-1)^2(\beta(\beta-1)(\lambda-1)-\alpha)}. \tag{3.11}$$

This measure indicates over-dispersion when IOD > 1, equi-dispersion when IOD $= 1$, and under-dispersion when IOD < 1. Another useful quantity is the zero-modification index (ZMI), defined relative to the Poisson baseline. Positive values indicate zero inflation, negative values indicate zero deflation, and zero indicates no zero-modification. For the DRLE distribution, the ZMI is given in the form

$$\text{ZMI} = 1 + \frac{\log[f(0;\alpha,\beta)]}{\mu_1'} = 1 + \frac{\beta(1-\beta)(\lambda-1)^2\log\left(\lambda\left(\frac{\alpha}{\beta-\beta^2}-1\right)+1\right)}{\lambda(\beta(\beta-1)(\lambda-1)-\alpha)}. \tag{3.12}$$

Remark 4. Table 1 and Figures 3–6 show that, for fixed β, increasing α substantially reduces the mean, variance, and index of dispersion, driving the distribution toward near-equidispersion while markedly reducing the zero-modification index. Skewness and kurtosis remain comparatively stable over this range, indicating that α primarily governs dispersion and zero-inflation rather than overall shape. In contrast, for fixed α, increasing β jointly increases the mean, variance, dispersion, zero-inflation, skewness, and kurtosis, indicating that β amplifies dispersion and tail heaviness. Across the parameter space considered, skewness and kurtosis values remain consistently above those expected under equidispersed or symmetric count models, confirming that the DRLE distribution retains pronounced right-skewness and heavy tails throughout. These complementary roles of α and β underscore the flexibility of the DRLE distribution in accommodating over-dispersed, zero-inflated, and heavy-tailed count data.

Table 1. Descriptive statistics of the DRLE distribution.

β	α	μ'_1	μ'_2	μ'_3	μ'_4	$V(X)$	IOD	ZMI	S.K	K.U
2	0.05	79.5000	9520.33	1.52×10^6	3.04×10^8	3200.08	40.2526	0.8983	1.4142	5.9998
	0.10	39.5000	2360.333	188440	1.88×10^7	800.083	20.2553	0.8299	1.4139	5.9994
	0.50	7.5000	88.3328	1399.75	27832.2	32.0821	4.2776	0.5159	1.4089	5.9846
	1.00	3.5003	20.3310	159.75	1580.2	8.0786	2.3079	0.3127	1.3950	5.9405
	3.00	0.8418	1.6439	4.2137	13.675	0.9353	1.1111	0.0306	1.3878	5.6811
2.5	0.05	82.8339	11583.7	2.23×10^6	5.46×10^8	4722.21	57.01	0.9396	1.5123	6.3426
	0.10	41.1678	2875.33	276910	3.38×10^7	1180.55	28.6765	0.8956	1.5123	6.3427
	0.50	7.8389	108.661	2083.09	50725.2	47.2126	6.0229	0.6645	1.5139	6.3450
	1.00	3.6779	25.3217	241.43	2929.36	11.7950	3.2070	0.4859	1.5190	6.3530
	3.00	0.9244	2.1467	6.7216	26.8836	1.2921	1.3977	0.1549	1.5988	6.4960
3	0.05	89.5007	14310.3	3.22×10^6	9.27×10^8	6299.96	70.39	0.9465	1.6199	6.7959
	0.10	44.5014	3555.33	399645	5.75×10^7	1574.96	35.3912	0.9079	1.6199	6.7962
	0.50	8.5069	135.33	3032.75	87111.2	62.9582	7.4008	0.7074	1.6222	6.8021
	1.00	4.0139	31.82	355.26	5089.69	15.7079	3.9134	0.5497	1.6294	6.8209
	3.00	1.0423	2.7913	10.2785	48.6844	1.7049	1.6357	0.2300	1.7137	7.0474
5	0.05	124.5010	29875.3	1.05×10^7	4.78×10^9	14374.9	115.461	0.9607	1.8313	7.8885
	0.10	62.0012	7437.83	1.30×10^6	2.97×10^8	3593.68	57.9614	0.9322	1.8314	7.8887
	0.50	12.0062	287.83	10062.3	459588	143.677	11.9669	0.7815	1.8328	7.8938
	1.00	5.7625	69.071	1206.01	27518.9	35.8646	6.2238	0.6592	1.8374	7.9097
	3.00	1.6208	6.5474	37.9685	287.918	3.9206	2.4189	0.3847	1.8869	8.0842

4. Estimation methods

In this section, we develop classical and Bayesian inference procedures for the DRLE distribution. Let $X_1, \ldots, X_n$ be independent observations from $X \sim \text{DRLE}(\alpha, \beta)$ with PMF

$$f(x; \alpha, \beta) = \left[\left(1 + \frac{\alpha(x+1)}{\beta(\beta-1)}\right)\left(\frac{1-\lambda}{\lambda}\right) - \frac{\alpha}{\lambda\beta(\beta-1)} \right] \lambda^{x+1}, \quad x \in \mathbb{N}_0, \tag{4.1}$$

where $\alpha > 0$, $\beta \geq 2$, and $\lambda = \exp(-\alpha/\beta)$. For brevity, write $c_\beta = \beta(\beta - 1)$ and denote the observed sample by $\mathbf{x} = (x_1, \ldots, x_n)$.

4.1. Maximum likelihood estimation

The likelihood and log-likelihood functions for (α, β) are

$$L(\alpha, \beta \mid \mathbf{x}) = \prod_{i=1}^{n} f(x_i; \alpha, \beta), \qquad \ell(\alpha, \beta) = \sum_{i=1}^{n} \log f(x_i; \alpha, \beta).$$

Because $\lambda = \exp(-\alpha/\beta)$ depends nonlinearly on (α,β), the score equations do not admit closed-form solutions. Hence, the maximum likelihood estimator (MLE)

$$(\widehat{\alpha},\widehat{\beta}) = \arg \max_{\alpha>0,\beta\geq 2} \ell(\alpha,\beta)$$

is obtained numerically. To enforce the constraints and improve numerical stability, we optimize over the unconstrained parameters

$$u = \log\alpha \in \mathbb{R}, \qquad v = \log(\beta - 2) \in \mathbb{R}, \tag{4.2}$$

so that $\alpha = \exp(u)$ and $\beta = 2 + \exp(v)$. Let $\widehat{\boldsymbol{\theta}} = (\widehat{u},\widehat{v})^\top$ denote the maximizer in (u, v)-space (e.g., obtained via the L–BFGS–B algorithm), and let $H(\widehat{\boldsymbol{\theta}})$ be the observed Hessian of $-\ell$ with respect to (u, v) evaluated at $\widehat{\boldsymbol{\theta}}$.

Approximate standard errors for $(\widehat{\alpha},\widehat{\beta})$ are computed via the delta method. Specifically, the estimated covariance matrix is

$$\widehat{\Sigma} = J(\widehat{\boldsymbol{\theta}})\, H(\widehat{\boldsymbol{\theta}})^{-1}\, J(\widehat{\boldsymbol{\theta}})^\top, \tag{4.3}$$

where the Jacobian matrix is

$$J(\widehat{\boldsymbol{\theta}}) = \begin{bmatrix} \partial\alpha/\partial u & \partial\alpha/\partial v \\ \partial\beta/\partial u & \partial\beta/\partial v \end{bmatrix}_{\boldsymbol{\theta}=\widehat{\boldsymbol{\theta}}} = \begin{bmatrix} \widehat{\alpha} & 0 \\ 0 & e^{\widehat{v}} \end{bmatrix}.$$

Consequently, Wald-type $100(1-\gamma)\%$ confidence intervals are

$$\widehat{\alpha} \pm z_{1-\gamma/2}\sqrt{\widehat{\Sigma}_{11}}, \qquad \widehat{\beta} \pm z_{1-\gamma/2}\sqrt{\widehat{\Sigma}_{22}}.$$

Reasonable starting values for numerical optimization can be obtained from crude moment-based approximations or by fitting a simpler discrete exponential model and refining the estimates using the full DRLE likelihood.

4.2. Goodness-of-fit assessment

The goodness-of-fit of the proposed DRLE distribution is evaluated using classical discrepancy measures based on observed and expected frequencies. In particular, we employ the Pearson chi-square statistic and information-theoretic criteria to assess model adequacy.

The Pearson chi-square statistic is defined as

$$\chi^2 = \sum_{j=1}^{k} \frac{(O_j - E_j)^2}{E_j},$$

where O_j and E_j denote the observed and expected frequencies, respectively, and k is the number of distinct count categories. Under the null hypothesis that the DRLE model is correctly specified, the statistic approximately follows a chi-square distribution with $k - p - 1$ degrees of freedom, where p is the number of estimated parameters. For each dataset, the test statistic is computed and compared with the corresponding chi-square distribution to assess model adequacy. Models yielding small chi-square values together with large p-values are regarded as providing an adequate fit, while large statistics with small p-values indicate significant lack of fit.

4.3. Bayesian inference

For Bayesian estimation, we assign weakly informative priors that respect the parameter constraints. Specifically, we assume independent Gamma priors under the shape–rate parameterization:

$$\alpha \sim \mathrm{Ga}(a_\alpha, b_\alpha), \qquad \beta - 2 \sim \mathrm{Ga}(a_\beta, b_\beta),$$

so that $\beta = 2 + W$ with $W \sim \mathrm{Ga}(a_\beta, b_\beta)$.

Let $(u, v) = (\log \alpha, \log(\beta - 2))$ as in (4.2). The posterior density in the transformed space is given by

$$\pi(u, v \mid \mathbf{x}) \propto L(\alpha(u), \beta(v) \mid \mathbf{x})\, \alpha(u)^{a_\alpha - 1} e^{-b_\alpha \alpha(u)}\, (\beta(v) - 2)^{a_\beta - 1} e^{-b_\beta(\beta(v)-2)}\, e^{u+v}, \tag{4.4}$$

where $\alpha(u) = e^u$, $\beta(v) = 2 + e^v$, and e^{u+v} is the Jacobian term.

Since the full conditional distributions are not of standard form, we implement a random-walk Metropolis–Hastings (RW–MH) algorithm on (u, v). At iteration ℓ, propose

$$u^\star = u^{(\ell)} + \varepsilon_u, \qquad v^\star = v^{(\ell)} + \varepsilon_v,$$

with $(\varepsilon_u, \varepsilon_v)^\top \sim N_2(\mathbf{0}, \Sigma_q)$. The proposal is accepted with probability

$$\min\left\{1,\ \frac{\pi(u^\star, v^\star \mid \mathbf{x})}{\pi(u^{(\ell)}, v^{(\ell)} \mid \mathbf{x})}\right\},$$

where $\pi(\cdot, \cdot \mid \mathbf{x})$ is given in (4.4). Posterior point estimates are taken as posterior means (or medians), and $100(1-\xi)\%$ credible intervals are computed from the empirical $\xi/2$ and $1-\xi/2$ posterior quantiles. Convergence is assessed using trace plots, autocorrelation diagnostics, and effective sample sizes (see, e.g., [7, 9, 13, 18]).

5. Numerical simulation

In this section, we present a comprehensive Monte Carlo simulation study to evaluate the finite-sample performance of the proposed DRLE distribution under maximum likelihood (MLE) and Bayesian estimation methods. All simulations are carried out in R version 4.3.0. Two parameter settings are considered:

$$(\alpha, \beta) = (1.2, 3.0) \quad \text{and} \quad (\alpha, \beta) = (1.8, 4.0),$$

representing two different scenarios for assessing the robustness of the estimation procedures.

The simulation study is conducted according to the following steps:

(1) Generate random samples from the proposed DRLE distribution under the selected parameter settings.
(2) Consider sample sizes
$$n = 50, 150, 250, 350, \text{ and } 400.$$
(3) Repeat the experiment for $M = 100$ Monte Carlo replications for each combination of parameter values and sample sizes.
(4) Compute the maximum likelihood and Bayesian estimates for every generated sample.

(5) Evaluate the estimation performance using Bias, Relative Bias (RelBias), Mean Squared Error (MSE), Root Mean Squared Error (RMSE), empirical coverage probabilities, interval lengths, and computational performance measures.

For the MLE approach, numerical optimization is performed using the L-BFGS-B algorithm, and convergence is assessed through the proportion of successful optimizations. Bayesian inference is implemented using the Random Walk Metropolis–Hastings algorithm. Posterior convergence is evaluated using trace plots, effective sample size (ESS), Monte Carlo standard error (MCSE), the Gelman–Rubin diagnostic ($\hat{R}$), and acceptance rates.

The Monte Carlo performance measures are defined as

$$\text{Bias} = \frac{1}{M}\sum_{i=1}^{M}(\hat{\theta}_i - \theta), \quad \text{RelBias} = \frac{1}{M}\sum_{i=1}^{M}\left(\frac{\hat{\theta}_i - \theta}{\theta}\right), \text{MSE} = \frac{1}{M}\sum_{i=1}^{M}(\hat{\theta}_i - \theta)^2, \quad \text{and} \quad \text{RMSE} = \sqrt{\text{MSE}},$$

where M denotes the number of Monte Carlo replications.

For Bayesian estimation, posterior interval performance is assessed using equal-tail and highest posterior density (HPD) credible intervals together with their empirical coverage probabilities and interval lengths. The MCMC algorithm is further evaluated through ESS, MCSE, MCSE/SD ratios, acceptance rates, and Gelman–Rubin $\hat{R}$ statistics to verify convergence and sampling efficiency.

Scenario 1: $\alpha = 1.2, \beta = 3.0$

Table 2 reports the probability mass function (PMF), cumulative distribution function (CDF), survival function, and hazard function of the proposed distribution for $\alpha = 1.2$ and $\beta = 3.0$. The PMF exhibits a monotonically decreasing pattern, with the highest probability occurring at $x = 0$ (0.195616). Thereafter, the probability gradually decreases, indicating that the distribution assigns greater probability to smaller count values while maintaining a relatively long right tail.

The cumulative distribution function increases smoothly toward one, reaching approximately 0.8004 at $x = 5$, 0.9451 at $x = 9$, and 0.9988 at $x = 20$. Consequently, the corresponding survival probabilities decrease from 0.8044 to 0.0012, demonstrating that the probability of observing values larger than x rapidly diminishes as x increases. Furthermore, the hazard function increases steadily from 0.1956 at $x = 0$ to 0.3029 at $x = 20$. This monotone increasing behavior indicates an increasing failure rate (IFR), implying that the conditional probability of occurrence at the next discrete time point becomes larger as the process evolves. Such a characteristic is particularly desirable for modeling lifetime and reliability data in which the risk of failure accumulates over time. Overall, these numerical results confirm that, under Scenario 1 ($\alpha = 1.2, \beta = 3.0$), the proposed distribution provides a right-skewed probability structure together with an increasing hazard rate, making it suitable for modeling discrete lifetime phenomena with ageing effects.

Table 2. PMF, CDF, survival and hazard function values of the proposed distribution.

x	PMF	CDF	Survival	Hazard
0	0.1956	0.1956	0.8044	0.1956
1	0.1753	0.3709	0.6291	0.2179
2	0.1472	0.5181	0.4819	0.2339
3	0.1185	0.6366	0.3634	0.2459
4	0.0927	0.7293	0.2707	0.2552
5	0.0711	0.8004	0.1996	0.2627
6	0.0536	0.8541	0.1459	0.2687
7	0.0399	0.8940	0.1059	0.2738
8	0.0295	0.9235	0.0765	0.2781
9	0.0216	0.9451	0.0549	0.2818
10	0.0157	0.9607	0.0393	0.2849
11	0.0113	0.9720	0.0279	0.2878
12	0.0081	0.9801	0.0199	0.2903
13	0.0058	0.9859	0.0141	0.2924
14	0.0041	0.9901	0.0099	0.2944
15	0.0029	0.9930	0.0069	0.2962
16	0.0021	0.9951	0.0049	0.2978
17	0.0015	0.9966	0.0034	0.2992
18	0.0010	0.9976	0.0024	0.3005
19	0.0007	0.9983	0.0017	0.3018
20	0.0005	0.9988	0.0012	0.3029

Figure 7 illustrates the probability mass function (PMF) and cumulative distribution function (CDF) of the proposed DRLE distribution for the parameter setting $\alpha = 1.2$ and $\beta = 3.0$. The left panel shows that the PMF attains its maximum at $x = 0$ and decreases monotonically as x increases, indicating that smaller count values occur with higher probability, while larger observations become progressively less likely. This behavior reflects a positively skewed discrete distribution with a relatively light right tail. The right panel presents the corresponding CDF, which increases monotonically toward one. A substantial proportion of the cumulative probability is accumulated within the first few integer values, after which the curve gradually approaches its limiting value. The rapid convergence of the CDF to one confirms that the probability of observing large counts becomes negligible for moderate values of x. Together, the PMF and CDF demonstrate that, under Scenario 1, the proposed DRLE distribution effectively models discrete data concentrated around small observations while retaining a sufficiently flexible tail behavior for larger values.

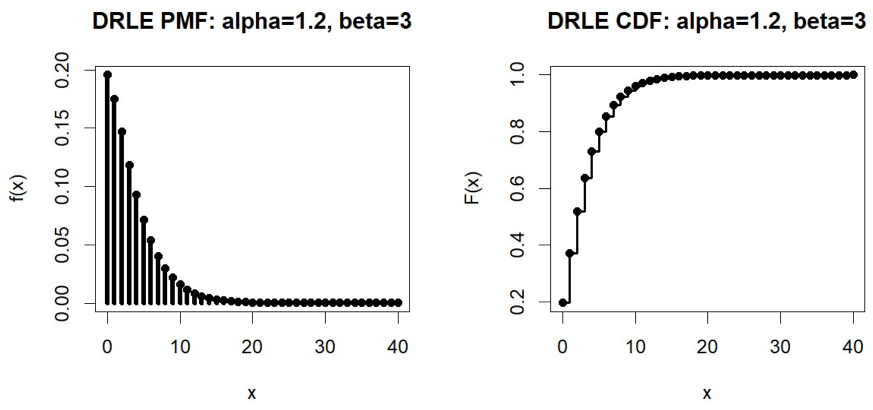

Figure 7. The PMF (left panel) and the CDF (right panel) of the proposed DRLE distribution for Scenario 1 with $\alpha = 1.2$ and $\beta = 3.0$.

Tables 3 and 4 present the maximum likelihood estimation results for Scenario 1, where the true parameter values are $\alpha = 1.2$ and $\beta = 3.0$. The numerical optimization procedure successfully converges in all 100 Monte Carlo replications for every sample size, resulting in a convergence rate of one. Nevertheless, successful numerical convergence does not necessarily imply accurate parameter estimation. For small and moderate sample sizes, the ML estimators exhibit substantial positive bias and large estimation errors. At $n = 50$, the average estimates of α and β are 7.082455 and 24.826450, respectively, which are considerably larger than their true values. The corresponding relative biases are 4.902046 and 7.275483, while the MSE values are 372.788418 and 5281.322004. These results indicate severe overestimation and considerable variability of the ML estimators for small samples.

Table 3. Monte Carlo simulation results for the maximum likelihood estimators under Scenario 1 with true parameter values $\alpha = 1.2$ and $\beta = 3.0$.

n	Parameter	True value	MLE	Bias	Relative bias	MSE	RMSE
50	α	1.2	7.0825	5.8825	4.9021	372.7884	19.3077
50	β	3.0	24.8265	21.8265	7.2755	5281.3220	72.6727
150	α	1.2	2.7864	1.5864	1.3219	78.4168	8.8553
150	β	3.0	8.8383	5.8383	1.9461	1127.4499	33.5775
250	α	1.2	2.1575	0.9575	0.7979	66.6861	8.1662
250	β	3.0	6.4459	3.4459	1.1487	871.9694	29.5291
350	α	1.2	1.2615	0.0615	0.0513	0.0429	0.2072
350	β	3.0	3.2457	0.2457	0.0819	0.6541	0.8088
400	α	1.2	1.4571	0.2571	0.2143	5.9442	2.4381
400	β	3.0	3.9999	0.9999	0.3333	86.3159	9.2906

Table 4. Coverage probabilities, confidence-interval characteristics, and convergence results of the maximum likelihood estimators under Scenario 1.

n	Parameter	Coverage$_{95\%}$	Lower	Upper	Length	Successful fits	Convergence rate
50	α	0.95	0.5222	757.1078	756.5857	100	1.00
50	β	0.84	2.0000	2818.3429	2816.3429	100	1.00
150	α	0.96	0.8002	123.3899	122.5897	100	1.00
150	β	0.89	2.0000	461.3804	459.3804	100	1.00
250	α	0.95	0.8609	76.1370	75.2760	100	1.00
250	β	0.91	2.0207	274.1963	272.1756	100	1.00
350	α	0.94	0.9039	1.6403	0.7364	100	1.00
350	β	0.93	2.1002	4.7205	2.6203	100	1.00
400	α	0.93	0.9597	20.1815	19.2217	100	1.00
400	β	0.93	2.1572	74.9729	72.8158	100	1.00

As the sample size increases from 50 to 350, the estimation performance improves substantially. In particular, at $n = 350$, the estimates of α and β become 1.261500 and 3.245742, which are close to the true parameter values. The corresponding relative biases decrease to 0.051250 and 0.081914, whereas the MSE values decline to 0.042935 and 0.654097, respectively. Therefore, the best ML estimation performance among the considered sample sizes is observed at $n = 350$.

However, the results at $n = 400$ do not preserve the expected improvement. The MSE values increase to 5.944211 for α and 86.315877 for β, and the confidence intervals become considerably wider than those obtained at $n = 350$. This non-monotonic behavior suggests that a small number of extreme estimates may have strongly affected the Monte Carlo averages. It may also indicate numerical instability, weak parameter identifiability, sensitivity to starting values, or convergence to local maxima of the likelihood function.

The empirical coverage probabilities generally range from 0.84 to 0.96. Although several coverage values are close to the nominal level of 0.95, the confidence intervals are extremely wide for $n = 50$, 150, and 250. Hence, the apparently satisfactory coverage at these sample sizes is mainly associated with imprecise intervals rather than accurate estimation. The intervals become substantially narrower at $n = 350$, consistent with the lower bias and MSE values observed at this sample size. Overall, the results show that the ML estimation procedure is numerically convergent but statistically unstable under some sample sizes for Scenario 1. Thus, the current findings do not provide clear evidence of a monotonic improvement in estimation accuracy as the sample size increases. Additional checks based on multiple starting values, parameter transformations, profile-likelihood analysis, and the examination of extreme Monte Carlo estimates are recommended to assess the reliability of the ML estimation procedure.

Tables 5–7 summarize the Bayesian estimation results for Scenario 1 with true parameter values $\alpha = 1.2$ and $\beta = 3.0$. Overall, the Bayesian estimators exhibit stable estimation behavior across all sample sizes. Unlike the maximum likelihood estimators, no severe overestimation is observed, and both parameters remain relatively close to their true values even for the smallest sample size. The estimation accuracy improves steadily as the sample size increases. For parameter α, the posterior mean decreases from 1.477175 at $n = 50$ to 1.311522 at $n = 400$, while the bias decreases from 0.277175 to 0.111522. Similarly, the MSE decreases from 0.117495 to 0.031190, indicating a substantial improvement in estimation precision. The same pattern is observed for β, whose bias decreases from 0.967607 to 0.462951, whereas the MSE declines from 1.167654 to 0.478987. These results suggest that the Bayesian estimators become increasingly accurate as more information is available.

Table 5. Monte Carlo simulation results for the Bayesian estimators under Scenario 1 with true parameter values $\alpha = 1.2$ and $\beta = 3.0$.

n	Parameter	True value	Bayes	Bias	Relative bias	MSE	RMSE
50	α	1.2	1.4772	0.2772	0.2309	0.1175	0.3428
50	β	3.0	3.9676	0.9676	0.3225	1.1677	1.0806
150	α	1.2	1.3800	0.1800	0.1500	0.0586	0.2421
150	β	3.0	3.8079	0.8079	0.2693	1.0784	1.0385
250	α	1.2	1.3821	0.1821	0.1518	0.0572	0.2391
250	β	3.0	3.6986	0.6986	0.2329	0.8539	0.9241
350	α	1.2	1.3551	0.1551	0.1293	0.0538	0.2320
350	β	3.0	3.6435	0.6435	0.2145	0.8149	0.9028
400	α	1.2	1.3115	0.1115	0.0929	0.0312	0.1766
400	β	3.0	3.4629	0.4629	0.1543	0.4789	0.6921

Table 6. Bayesian interval estimation results under Scenario 1.

n	Parameter	Equal-tail cov.	HPD cov.	Equal-tail lower	Equal-tail upper	Equal-tail length	HPD Lower	HPD upper	HPD length
50	α	0.98	0.99	0.9851	2.3973	1.4122	0.9149	2.2204	1.3055
50	β	0.99	1.00	2.3948	7.2269	4.8322	2.2024	6.5086	4.3062
150	α	0.97	1.00	1.0309	2.0879	1.0570	0.9774	1.9351	0.9577
150	β	0.96	0.99	2.5206	6.5741	4.0535	2.3545	5.9498	3.5954
250	α	0.91	0.99	1.0803	2.0142	0.9339	1.0307	1.8703	0.8396
250	β	0.97	0.99	2.57718	6.1563	3.5791	2.4157	5.5819	3.1662
350	α	0.89	0.95	1.0888	1.9084	0.8197	1.0474	1.7825	0.7351
350	β	0.91	0.96	2.6364	5.8332	3.1968	2.4832	5.3148	2.8316
400	α	0.93	0.97	1.0829	1.7891	0.7062	1.0439	1.6752	0.6312
400	β	0.93	0.98	2.5962	5.3632	2.7670	2.4655	4.9033	2.4378

Table 7. Acceptance rates of the Random Walk Metropolis–Hastings algorithm.

n	Parameter	Acceptance rate	Successful fits
50	α	0.5397	100
50	β	0.5397	100
150	α	0.3741	100
150	β	0.3741	100
250	α	0.3030	100
250	β	0.3030	100
350	α	0.2596	100
350	β	0.2596	100
400	α	0.2433	100
400	β	0.2433	100

The interval estimation results also support the reliability of the Bayesian procedure. The equal-tail and HPD credible intervals achieve empirical coverage probabilities close to the nominal 95% level. In addition, the interval lengths decrease monotonically with increasing sample size, reflecting the reduction in posterior uncertainty. The HPD intervals are consistently shorter than the corresponding equal-tail intervals, demonstrating their greater efficiency while maintaining comparable coverage probabilities. The Random Walk Metropolis–Hastings algorithm converged successfully for all Monte Carlo replications. The acceptance rates decrease gradually from approximately 0.54 at $n = 50$ to 0.24 at $n = 400$, remaining within acceptable ranges for efficient MCMC sampling. Furthermore, all simulation runs are completed successfully, indicating stable computational performance of the Bayesian estimation procedure. Overall, the Bayesian estimation method demonstrates accurate, stable, and robust finite-sample performance for the proposed DRLE distribution. Compared with the corresponding maximum likelihood results, the Bayesian estimators exhibit considerably smaller bias and MSE values, narrower interval estimates, and more consistent behavior across sample sizes, making the Bayesian approach the preferable estimation method for Scenario 1.

Figures 8–10 provide a comprehensive comparison of the maximum likelihood (MLE) and Bayesian estimation procedures under Scenario 1. As shown in Figure 8, the Bayesian estimator consistently produces substantially smaller mean squared error (MSE) values than the MLE estimator for both parameters across all sample sizes. Although the MSE values generally decrease as the sample size increases, the MLE estimator exhibits extremely large estimation errors for small samples and a noticeable increase at $n = 400$, particularly for the parameter β. In contrast, the Bayesian estimator displays a smooth and monotonic reduction in MSE, demonstrating superior numerical stability and estimation accuracy.

The point estimation results shown in Figure 9 further support these findings. For small sample sizes, the MLE estimates considerably overestimate both parameters and remain far from their true values. As the sample size increases, the MLE estimates gradually approach the true parameter values; however, a slight deterioration is observed at $n = 400$. By comparison, the Bayesian estimates remain consistently close to the true parameter values throughout the entire range of sample sizes, exhibiting substantially smaller bias and a much more stable estimation behavior.

The interval estimation results presented in Figure 10 also favor the Bayesian approach. The MLE confidence intervals are extremely wide for small sample sizes, reflecting the considerable uncertainty associated with the corresponding point estimates. Although these intervals become shorter as the sample size increases, they remain highly variable. In contrast, the Bayesian equal-tail and highest posterior density (HPD) credible intervals are consistently shorter and decrease steadily as more observations become available. Furthermore, the HPD intervals are uniformly shorter than the corresponding equal-tail intervals while maintaining similar empirical coverage probabilities, indicating greater efficiency in posterior uncertainty quantification. Overall, the graphical evidence consistently demonstrates that the Bayesian estimation procedure provides more accurate point estimates, smaller estimation errors, and considerably more efficient interval estimates than the classical MLE approach. Under the considered parameter setting, the Bayesian method therefore represents the more reliable and robust estimation procedure for the proposed DRLE distribution.

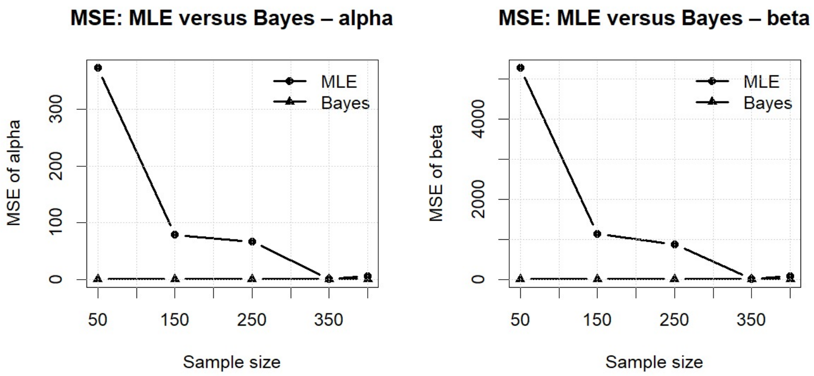

Figure 8. Comparison of the MSE values of the MLE and Bayesian estimators for the parameters α and β under Scenario 1 ($\alpha = 1.2, \beta = 3.0$).

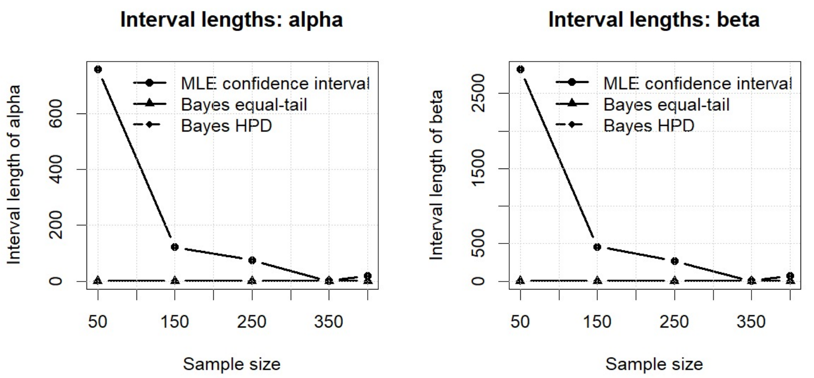

Figure 9. Comparison of the MLE and Bayesian point estimates together with the true parameter values for α and β under Scenario 1.

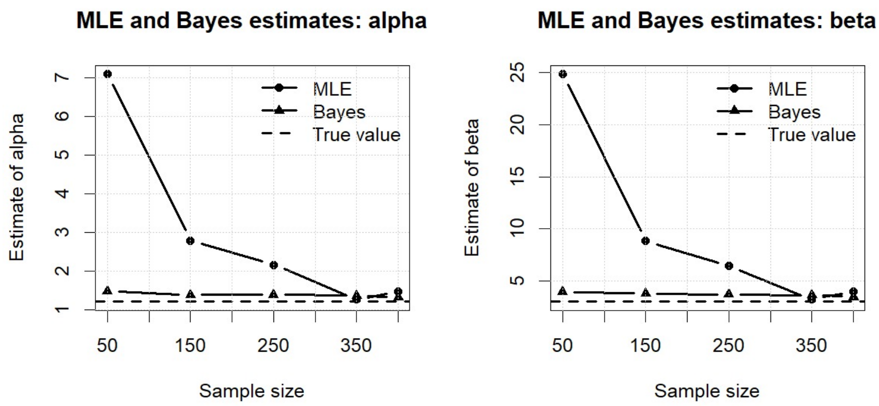

Figure 10. Comparison of interval lengths for the MLE confidence intervals and the Bayesian equal-tail and HPD credible intervals under Scenario 1.

Overall, Figures 8–10 consistently demonstrate the advantages of the Bayesian estimation procedure over the classical maximum likelihood approach. The Bayesian method yields smaller estimation errors, parameter estimates that remain closer to the true values, and substantially shorter interval estimates. In contrast, the MLE procedure exhibits considerable instability for small sample sizes and non-monotonic behavior for the largest sample size considered, suggesting sensitivity to the optimization process and possible local maxima of the likelihood function. Consequently, under Scenario 1, the Bayesian approach provides a more reliable and robust estimation framework for the proposed DRLE distribution.

Table 8 summarizes the Markov chain Monte Carlo (MCMC) diagnostic measures for the Bayesian estimation procedure under Scenario 1. The posterior means of the parameters are 1.244626 for α and 2.981389 for β, which are close to their corresponding true values ($\alpha = 1.2$ and $\beta = 3.0$), indicating satisfactory posterior estimation accuracy. The effective sample sizes (ESS) are approximately 511 for α and 432 for β, suggesting that the Markov chains contain a sufficiently large number of effectively independent samples for reliable posterior inference. The Monte Carlo standard errors (MCSE) are very small relative to the corresponding posterior standard deviations, with MCSE/SD ratios equal to 0.044222 for α and 0.048106 for β. Since both ratios are well below the commonly accepted threshold of 0.10, the Monte Carlo error is negligible relative to the posterior uncertainty, indicating that the simulation length is adequate. Furthermore, the Random Walk Metropolis–Hastings algorithm achieves an acceptance rate of approximately 27.9% for both parameters, which lies within the generally recommended range for efficient MCMC sampling. Overall, the diagnostic measures indicate good mixing, stable posterior estimation, and satisfactory convergence of the Markov chains, supporting the reliability of the Bayesian estimation results. Table 9 reports the Gelman–Rubin convergence diagnostic for the Bayesian MCMC algorithm. The estimated potential scale reduction factors are $\hat{R} = 1.005562$ for α and $\hat{R} = 1.004993$ for β, with upper confidence limits of 1.006477 and 1.005632, respectively. Since all $\hat{R}$ values and their corresponding upper confidence limits are extremely close to 1, there is no evidence of lack of convergence among the parallel Markov chains. These results indicate that the between-chain and within-chain variances are nearly identical, suggesting satisfactory mixing and convergence of the MCMC algorithm. Therefore, the posterior samples can be regarded as reliable for Bayesian inference, providing additional support for the validity of the posterior estimates and credible intervals reported in the simulation study.

Table 8. MCMC diagnostic measures for the Bayesian estimation procedure under Scenario 1 ($\alpha = 1.2, \beta = 3.0$).

Parameter	Posterior mean	Posterior SD	ESS	MCSE	MCSE/SD	Acceptance rate
α	1.2446	0.1416	511.3573	0.0063	0.0442	0.2788
β	2.9814	0.5438	432.1245	0.0262	0.0481	0.2789

Table 9. Gelman–Rubin convergence diagnostic ($\hat{R}$) for the Bayesian MCMC algorithm under Scenario 1 ($\alpha = 1.2, \beta = 3.0$).

Parameter	$\hat{R}$	Upper CI
α	1.0056	1.0065
β	1.0049	1.0056

Figure 11 presents the MCMC diagnostic plots for Scenario 1 with the true parameter values $\alpha = 1.2$ and $\beta = 3.0$. The trace plots (left panels) indicate that both Markov chains fluctuate randomly around stable posterior means without exhibiting noticeable trends or systematic drifts, providing evidence of satisfactory convergence and good mixing. The chains visit the entire high-density posterior region throughout the simulation, suggesting that the sampling algorithm efficiently explores the posterior distributions.

The posterior histograms (right panels) further confirm these findings. Both posterior distributions are unimodal and centered close to the true parameter values. The posterior distribution of α is tightly concentrated around 1.2, while that of β is centered near 3.0. Although both distributions display a slight right skewness, the majority of the posterior probability mass remains close to the true parameter values, indicating accurate parameter recovery. The dashed vertical lines represent the 95% credible intervals, whereas the solid vertical line denotes the posterior mean. Overall, the diagnostic plots demonstrate that the Bayesian estimation procedure provides stable posterior samples and reliable parameter estimates for Scenario 1.

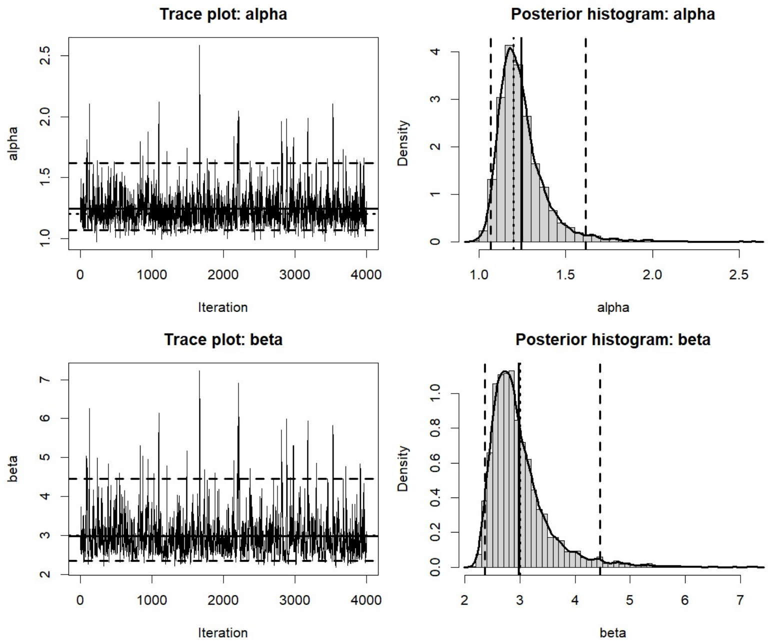

Figure 11. MCMC diagnostic plots for Scenario 1 ($\alpha = 1.2$, $\beta = 3.0$). The left panels display the trace plots of the posterior samples for α and β, while the right panels present the corresponding posterior histograms with posterior means (solid vertical lines) and 95% credible intervals (dashed vertical lines).

Scenario 2: $\alpha = 1.8, \beta = 4.0$

Table 10 presents the probability mass function (PMF), cumulative distribution function (CDF), survival function, and hazard function of the proposed DRLE distribution under Scenario 2 with $\alpha = 1.8$ and $\beta = 4.0$. The PMF exhibits a strictly decreasing pattern, with the highest probability occurring at $x = 0$ (0.266728). Thereafter, the probability decreases steadily, indicating that the distribution places most of its probability mass on smaller count values while retaining a gradually decaying right tail. The cumulative distribution function increases monotonically toward one, reaching approximately 0.8156 at $x = 4$, 0.9122 at $x = 6$, and 0.9997 at $x = 20$. Consequently, the survival probabilities decrease rapidly from 0.7333 at $x = 0$ to only 0.0003 at $x = 20$, showing that the probability of observing values larger than 20 is practically negligible.

The hazard function displays a clear monotonic increasing pattern, rising from 0.266728 at $x = 0$ to 0.338461 at $x = 20$. This behavior indicates an increasing failure rate (IFR), implying that the conditional probability of failure at the next discrete time point increases as time progresses. Compared with Scenario 1, the hazard values are consistently larger over the entire support, indicating a stronger ageing effect under the parameter combination $\alpha = 1.8$ and $\beta = 4.0$. Overall, the numerical results demonstrate that the proposed DRLE distribution under Scenario 2 is positively skewed, possesses a rapidly increasing cumulative probability, and exhibits a stable increasing hazard function. These characteristics make the model particularly suitable for analysing discrete lifetime and reliability data in which failures become progressively more likely as the process evolves.

Table 10. PMF, CDF, survival and hazard function values of the proposed DRLE distribution under Scenario 2 ($\alpha = 1.8, \beta = 4.0$).

x	PMF	CDF	Survival	Hazard
0	0.2667	0.2667	0.7333	0.2667
1	0.2047	0.4715	0.5285	0.2792
2	0.1526	0.6241	0.3759	0.2888
3	0.1114	0.7355	0.2645	0.2964
4	0.0800	0.8156	0.1845	0.3026
5	0.0568	0.8723	0.1277	0.3077
6	0.0398	0.9122	0.0879	0.3120
7	0.0277	0.9399	0.0601	0.3157
8	0.0192	0.9591	0.0409	0.3189
9	0.0132	0.9722	0.0278	0.3217
10	0.0090	0.9812	0.0188	0.3241
11	0.0061	0.9874	0.0127	0.3263
12	0.0042	0.9915	0.0085	0.3282
13	0.0028	0.9943	0.0057	0.3299
14	0.0019	0.9962	0.0038	0.3315
15	0.0013	0.9975	0.0025	0.3329
16	0.0009	0.9983	0.0017	0.3342
17	0.0006	0.9989	0.0011	0.3354
18	0.0004	0.9993	0.0008	0.3365
19	0.0003	0.9995	0.0005	0.3375
20	0.0002	0.9997	0.0003	0.3385

Figure 12 illustrates the probability mass function (PMF) and cumulative distribution function (CDF) of the proposed DRLE distribution for the parameter setting $\alpha = 1.8$ and $\beta = 4.0$. The left panel shows that the PMF reaches its maximum at $x = 0$ and decreases monotonically as x increases. Compared with Scenario 1, the probability mass is more strongly concentrated around the smallest count values, indicating that larger observations become increasingly unlikely under this parameter configuration. The rapid decline of the PMF also suggests a lighter right tail while preserving the flexibility required for modeling discrete lifetime data. The right panel presents the corresponding cumulative distribution function, which increases monotonically and approaches one more rapidly than in Scenario 1. Most of the cumulative probability is accumulated within the first few integer values, and the CDF is already very close to one for moderate values of x. This behavior indicates that the probability of observing large counts is negligible. Overall, the PMF and CDF demonstrate that the proposed DRLE distribution under Scenario 2 produces a positively skewed discrete distribution with probability mass concentrated at small counts and a rapidly increasing cumulative probability. These characteristics, together with the increasing hazard behavior observed in Table 10, indicate that the proposed distribution is well suited for modeling discrete lifetime and reliability data exhibiting a pronounced aging effect.

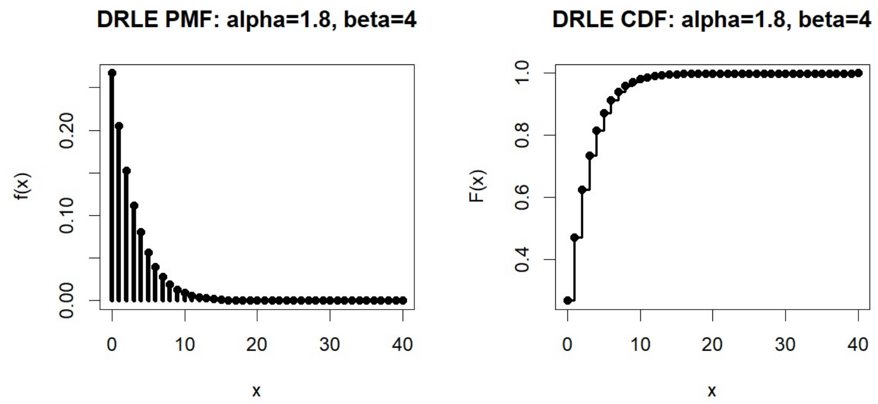

Figure 12. The PMF (left panel) and the CDF (right panel) of the proposed DRLE distribution for Scenario 2 with $\alpha = 1.8$ and $\beta = 4.0$.

The maximum likelihood estimation results for Scenario 2 are presented in Tables 11 and 12. The numerical optimization algorithm converged successfully in all Monte Carlo replications, yielding a convergence rate of one for every sample size. However, despite the successful convergence, the MLE procedure exhibits substantial estimation bias and extremely large estimation errors throughout the simulation study. For the smallest sample size ($n = 50$), the ML estimates are considerably larger than the corresponding true parameter values. Specifically, the average estimates are 20.104836 for α and 56.288646 for β, compared with the true values $\alpha = 1.8$ and $\beta = 4.0$. Consequently, the relative biases are 10.169354 and 13.072161, while the corresponding MSE values reach 2030.3438 and 16523.5786, respectively. These results indicate severe overestimation and substantial estimation variability for both parameters. Although the estimation accuracy generally improves as the sample size increases, the improvement is relatively slow. Even at $n = 400$, the average estimates remain noticeably larger than the true parameter values, with estimates of 5.589616 for α and 15.210429 for β. Likewise, the corresponding MSE values remain very large (332.0959 and 2919.4679), indicating that the MLE procedure still produces considerable estimation errors even for the largest sample size considered.

Table 11. Monte Carlo simulation results for the maximum likelihood estimators under Scenario 2 with true parameter values $\alpha = 1.8$ and $\beta = 4.0$.

n	Parameter	True value	MLE	Bias	Relative bias	MSE	RMSE
50	α	1.8	20.1048	18.3048	10.1694	2030.3438	45.0593
50	β	4.0	56.2887	52.2887	13.0722	16523.5786	128.5441
150	α	1.8	9.9494	8.1494	4.5274	886.8043	29.7793
150	β	4.0	27.7134	23.7134	5.9284	7673.4236	87.5981
250	α	1.8	13.0210	11.2210	6.2339	1082.3775	32.8995
250	β	4.0	36.6624	32.6624	8.1656	9189.0515	95.8596
350	α	1.8	8.6756	6.8756	3.8198	549.7550	23.4469
350	β	4.0	23.6936	19.6936	4.9234	4413.4212	66.4336
400	α	1.8	5.5896	3.7896	2.1053	332.0959	18.2235
400	β	4.0	15.2104	11.2104	2.8026	2919.4679	54.0321

Table 12. Coverage probabilities, confidence interval characteristics, and convergence results of the maximum likelihood estimators under Scenario 2.

n	Parameter	$\text{Coverage}_{95\%}$	Lower	Upper	Length	Successful fits	Convergence rate
50	α	0.85	0.4811	2481.8272	2481.3460	100	1.00
50	β	0.76	2.0000	7096.1395	7094.1395	100	1.00
150	α	0.92	0.6316	746.7090	746.0774	100	1.00
150	β	0.86	2.0000	2184.2895	2182.2895	100	1.00
250	α	0.84	0.6725	1021.7541	1021.0816	100	1.00
250	β	0.86	2.0029	2974.8384	2972.8355	100	1.00
350	α	0.86	0.7305	515.4448	514.7142	100	1.00
350	β	0.87	2.0289	1471.6112	1469.5824	100	1.00
400	α	0.89	0.848182	300.8792	300.0310	100	1.00
400	β	0.85	2.060415	886.4639	884.4035	100	1.00

The confidence interval results further support these findings. The empirical coverage probabilities vary approximately between 0.76 and 0.92, remaining below the nominal 95% confidence level in nearly all simulation settings. Moreover, the confidence intervals are extremely wide, particularly for small and moderate sample sizes. For example, the confidence interval length for β exceeds 7000 at $n = 50$ and remains above 880 even at $n = 400$, reflecting the high variability of the ML estimators. Overall, the results indicate that, under Scenario 2, the maximum likelihood estimation procedure suffers from substantial positive bias, large mean squared errors, and excessively wide confidence intervals. Although numerical convergence is achieved in all replications, the statistical performance of the MLE estimator remains unsatisfactory, suggesting that maximum likelihood estimation is not a reliable inferential procedure for the proposed DRLE distribution under this parameter configuration.

Tables 13–15 summarize the Bayesian estimation results under Scenario 2, where the true parameter values are $\alpha = 1.8$ and $\beta = 4.0$. The Bayesian estimators exhibit stable performance across all sample sizes, producing estimates that remain close to the corresponding true parameter values. In contrast to the maximum likelihood estimators, no severe overestimation is observed, even for the smallest sample size. For the parameter α, the posterior mean estimates range from 1.864005 to 1.933891, with absolute biases below 0.14 and MSE values between 0.039894 and 0.074285. Similarly, the Bayesian estimates of β remain close to the true value of 4.0, with relative biases below 0.11 and MSE values below 0.64 throughout the simulation study. These results indicate that the Bayesian procedure provides accurate and stable estimation even under moderate sample sizes.

The interval estimation results further demonstrate the reliability of the Bayesian approach. The empirical coverage probabilities of both the equal-tail and HPD credible intervals remain close to the nominal 95% level, generally ranging between 0.96 and 1.00. Moreover, the interval lengths decrease steadily as the sample size increases, reflecting the reduction in posterior uncertainty. The HPD credible intervals are consistently shorter than the corresponding equal-tail intervals while maintaining comparable coverage probabilities, indicating greater efficiency of the HPD intervals.

Table 13. Monte Carlo simulation results for the Bayesian estimators under Scenario 2 with true parameter values $\alpha = 1.8$ and $\beta = 4.0$.

n	Parameter	True value	Bayes	Bias	Relative bias	MSE	RMSE
50	α	1.8	1.8894	0.0894	0.0496	0.0743	0.2726
50	β	4.0	4.1138	0.1138	0.0285	0.2209	0.4701
150	α	1.8	1.8640	0.0640	0.0356	0.0399	0.1997
150	β	4.0	4.2651	0.2651	0.0663	0.4213	0.6491
250	α	1.8	1.9215	0.1215	0.0675	0.0608	0.2466
250	β	4.0	4.3112	0.3112	0.0778	0.4965	0.7046
350	α	1.8	1.9339	0.1339	0.0744	0.0738	0.2716
350	β	4.0	4.4109	0.4109	0.1027	0.6359	0.7975
400	α	1.8	1.8921	0.0921	0.0512	0.0462	0.2149
400	β	4.0	4.2744	0.2744	0.0686	0.4095	0.6399

Table 14. Bayesian interval estimation results under Scenario 2.

n	Parameter	Equal-tail Cov.	HPD Cov.	Equal-tail lower	Equal-tail upper	Equal-tail length	HPD Lower	HPD upper	HPD length
50	α	1.00	1.00	1.2553	3.0177	1.7623	1.1665	2.8128	1.6464
50	β	1.00	1.00	2.4857	7.2617	4.7760	2.2703	6.6067	4.3365
150	α	0.99	0.97	1.3489	2.8314	1.4824	1.2749	2.6392	1.3643
150	β	0.99	0.97	2.7321	7.2199	4.4879	2.5321	6.6105	4.0785
250	α	0.99	0.97	1.4344	2.8476	1.4132	1.3653	2.6664	1.3011
250	β	1.00	0.96	2.8579	7.1109	4.2530	2.6599	6.5375	3.8776
350	α	0.98	0.99	1.4631	2.8407	1.3776	1.3975	2.6569	1.2595
350	β	0.98	0.97	2.9733	7.1936	4.2203	2.7769	6.6136	3.8367
400	α	0.98	0.98	1.4559	2.7462	1.2903	1.3934	2.5689	1.1756
400	β	0.99	0.98	2.9362	6.9075	3.9712	2.7473	6.3478	3.6005

Table 15. Acceptance rates of the Random Walk Metropolis–Hastings algorithm under Scenario 2.

n	Parameter	Acceptance rate	Successful fits
50	α	0.5394	100
50	β	0.5394	100
150	α	0.3752	100
150	β	0.3752	100
250	α	0.3039	100
250	β	0.3039	100
350	α	0.2619	100
350	β	0.2619	100
400	α	0.2465	100
400	β	0.2465	100

The Random Walk Metropolis–Hastings algorithm performs satisfactorily throughout the simulation study. The acceptance rates decrease gradually from approximately 0.54 at $n = 50$ to 0.25 at $n = 400$, remaining within the commonly recommended range for efficient MCMC sampling. Furthermore, all Monte Carlo replications were completed successfully, resulting in a success rate of 100% for every sample size. Overall, the Bayesian estimation procedure provides accurate point estimates, small estimation errors, reliable credible intervals, and stable computational performance under Scenario 2. Compared with the corresponding maximum likelihood estimation results, the Bayesian approach yields substantially smaller bias and MSE values together with considerably narrower interval estimates, confirming its superior finite-sample performance for the proposed DRLE distribution.

Figures 13–15 provide a comprehensive comparison of the maximum likelihood (MLE) and Bayesian estimation procedures under Scenario 2. As illustrated in Figure 13, the Bayesian estimator consistently produces dramatically smaller mean squared error (MSE) values than the MLE estimator for both parameters across all sample sizes. The MLE procedure yields extremely large estimation errors, particularly for small and moderate sample sizes, and although the MSE values generally decrease as the sample size increases, they remain substantially larger than those of the Bayesian estimator even at $n = 400$. In contrast, the Bayesian estimator maintains relatively small and stable MSE values throughout the simulation study, demonstrating considerably greater estimation accuracy and numerical stability.

The point estimation results presented in Figure 14 further reinforce these findings. The MLE estimates substantially overestimate both parameters for every sample size considered and remain far from the corresponding true parameter values even for the largest sample size. Although some improvement is observed as the sample size increases, the MLE estimates continue to exhibit considerable positive bias. In contrast, the Bayesian estimates remain consistently close to the true parameter values across all sample sizes, showing only minor fluctuations and substantially smaller estimation bias.

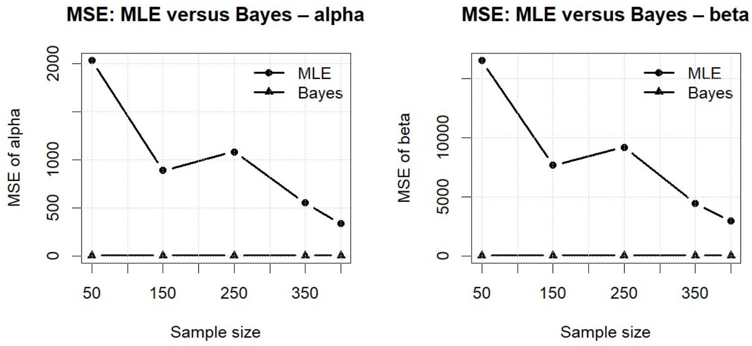

Figure 13. Comparison of the MSE values of the MLE and Bayesian estimators for the parameters α and β under Scenario 2 ($\alpha = 1.8, \beta = 4.0$).

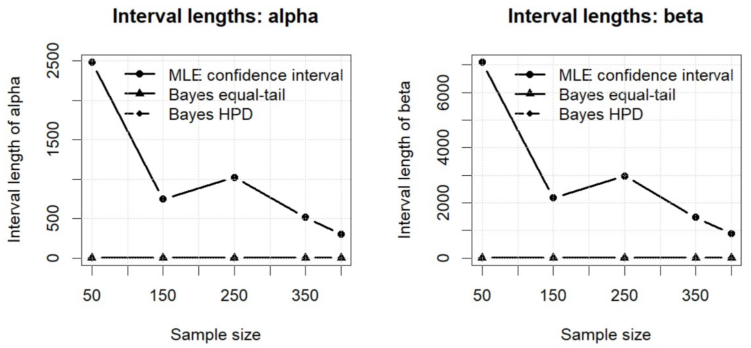

Figure 14. Comparison of the MLE and Bayesian point estimates together with the true parameter values for α and β under Scenario 2.

Figure 15 compares the interval lengths of the MLE confidence intervals with the Bayesian equal-tail and HPD credible intervals. The MLE intervals are substantially wider than the Bayesian intervals for all sample sizes, although all interval lengths decrease as the sample size increases. The HPD intervals are consistently shorter than the equal-tail intervals while providing similar empirical coverage, indicating greater efficiency. Overall, the Bayesian approach yields more accurate parameter estimates, smaller estimation errors, and markedly shorter credible intervals than the MLE under Scenario 2 ($\alpha = 1.8, \beta = 4.0$).

Figure 16 presents the MCMC trace plots and posterior distributions of the parameters α and β under Scenario 2. The trace plots fluctuate around stable regions without displaying any systematic trend, drift, or explosive behavior. This pattern suggests that the Markov chains have reached their stationary distributions and exhibit satisfactory mixing throughout the retained iterations. For parameter α, the posterior distribution is unimodal and slightly right-skewed, with most of the posterior mass concentrated around the true value $\alpha = 1.8$. Similarly, the posterior distribution of β is unimodal and positively skewed, with the main concentration of posterior probability located near the true value $\beta = 4.0$. The longer right tails observed in both posterior distributions indicate some posterior asymmetry, which is more pronounced for β.

The solid vertical lines represent the posterior point estimates, whereas the dotted vertical lines indicate the corresponding true parameter values. The dashed vertical lines show the lower and upper limits of the Bayesian credible intervals. In both cases, the true parameter values lie within the credible intervals, supporting the accuracy of the Bayesian estimation procedure. Overall, the trace plots and posterior histograms provide graphical evidence of satisfactory MCMC convergence, stable chain behavior, and adequate posterior estimation for both parameters under Scenario 2. These findings are consistent with the small bias and MSE values obtained from the Bayesian simulation results.

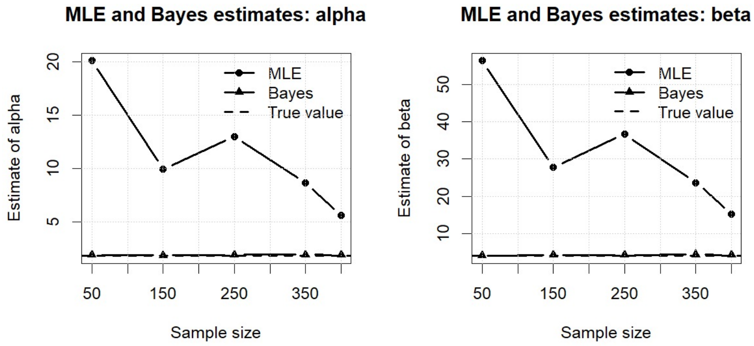

Figure 15. Comparison of interval lengths for the MLE confidence intervals and the Bayesian equal-tail and HPD credible intervals under Scenario 2.

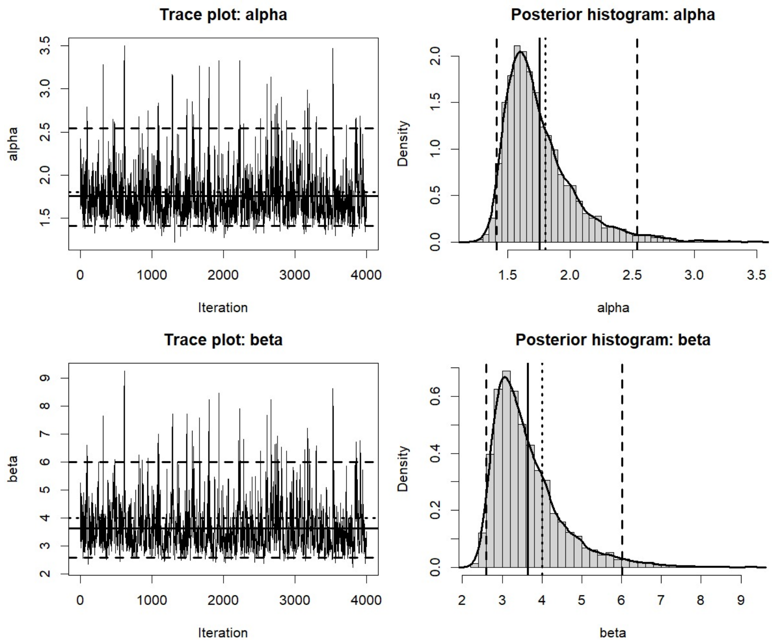

Figure 16. MCMC trace plots and posterior density histograms for the parameters α and β under Scenario 2 with true parameter values $\alpha = 1.8$ and $\beta = 4.0$. The left panels show the trace plots, whereas the right panels display the corresponding posterior histograms and kernel density estimates.

6. Applications and data analysis

In this section, we investigate the practical applicability and performance of the proposed DRLE distribution by analyzing several real-life datasets originating from different application areas. To demonstrate the flexibility and competitiveness of the DRLE model, its fit is compared with a number of well-established one-parameter and two-parameter discrete lifetime distributions that have been widely used in the recent literature.

Model comparison is carried out using likelihood-based and goodness-of-fit measures, including the negative log-likelihood ($-\ell$), Akaike Information Criterion (AIC), Bayesian Information Criterion (BIC), and the chi-square goodness-of-fit statistic (χ^2) along with its associated degrees of freedom (DF) and p-value. In general, smaller values of $-\ell$, AIC, BIC, and χ^2, accompanied by larger p-values, indicate a superior model fit.

Since the ordinary chi-square approximation is unreliable when expected cell frequencies are small, adjacent categories (starting from the largest observed value) are pooled together prior to computing the χ^2 statistic, so that each resulting category has an expected frequency of at least five. The degrees of freedom are adjusted accordingly as (number of pooled categories − number of estimated parameters − 1).

The competing discrete distributions considered in the analysis are summarized in Table 16. These models are selected due to their popularity, structural diversity, and proven performance in modeling discrete lifetime and count data.

Table 16. Competing discrete models for the DRLE distribution.

Models	**Abbreviation**	**Author(s)**
Exponentiated discrete lindley	EDL	[11]
Poisson moment exponential	Poi–MEx	[2]
Discrete moment exponential	DMEx	[1]
Discrete Ramos–Louzada	DRL	[10]
Poisson Ramos–Louzada	Poi–RL	[5]
Discrete rayleigh	DR	[19]
Discrete Burr–Hatke	DBH	[12]
Poisson	Poi	[17]

The information criteria employed in the comparison are defined as

$$\begin{aligned} \text{AIC} &= -2\log\ell + 2p, \\ \text{BIC} &= -2\log\ell + p\log(n), \end{aligned}$$

where n represents the sample size, and p is the number of model parameters. These criteria provide a trade-off between model goodness-of-fit and complexity, thereby facilitating an objective comparison among competing models.

6.1. Dataset I: European corn-borer larvae counts

Dataset I consists of biological experiment data representing the number of European corn-borer larvae (*pyrausta*) observed in corn fields, originally reported by Bodhisuwan and Sangpoom [8]. The experiment was conducted on eight hills with 15 replications, where the number of larvae per hill is recorded.

To explore the distributional characteristics of the data, nonparametric graphical tools, including boxplots, violin plots, and normal Q–Q plots, are employed. These exploratory summaries, displayed in Figure 17, provide preliminary insights into skewness, dispersion, and potential deviations from normality.

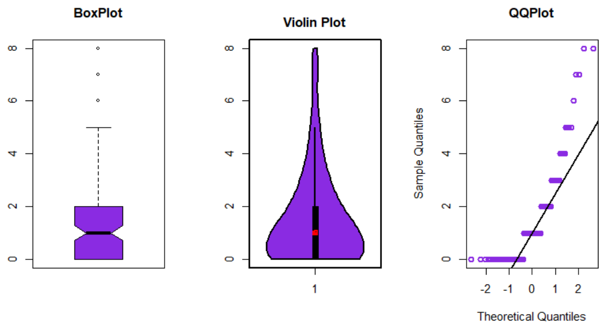

Figure 17. Nonparametric exploratory plots for Dataset I.

As shown in Table 17, the proposed DRLE model has the smallest negative log-likelihood ($-\ell$ = 200.415) among all fitted models, indicating the best overall fit to Dataset I. In fact, the single-parameter Poi-MEx model yields slightly lower AIC and BIC values due to the reduced penalty for the number of parameters. Nevertheless, DRLE and EDL achieve comparable values of the information criteria (AIC and BIC within 1 unit of Poi-MEx), with the added flexibility of a second parameter that allows the model to better capture the shape and dispersion of the data. This is further confirmed by Table 18, where DRLE provides the smallest chi-square statistic and the largest p-value among all competing models, confirming its better goodness of fit. Overall, DRLE has the best flex-fit trade-off for Dataset I and is recommended as the preferred model, with EDL and Poi-MEx as competitive alternatives.

Table 17. Parameter estimates and information criteria for the fitted models for data I.

Model $\downarrow$	$\hat{\alpha}$	$\hat{\beta}$	SE($\hat{\alpha}$)	SE($\hat{\beta}$)	-ℓ	AIC	BIC
DRLE	2.5002	3.4641	0.6998	1.4971	200.415	404.83	410.405
EDL	0.4693	0.9009	0.0421	0.1706	200.492	404.984	410.559
Poi-MEx	0.7416	-	0.1456	-	201.220	404.440	407.230
DMEx	0.9969	-	0.0656	-	205.476	412.952	415.740
DRL	2.5790	-	0.1839	-	238.009	478.018	480.805
Poi-RL	2.5243	-	0.1946	-	244.501	491.002	493.790
DR	0.8670	-	0.0115	-	235.230	472.450	475.240
DBH	0.8655	-	0.0385	-	214.049	430.098	432.885
Poi	1.483	-	0.025	-	219.190	440.380	443.160

Table 18. Goodness of fit statistics for Dataset I.

X	Observed	DRLE	EDL	Poi-MEx	DMEx	DRL	Poi-RL	DR	DBH	Poi
0	43	44.613	44.025	39.558	31.844	18.574	38.28	15.920	68.073	27.226
1	35	30.458	30.579	33.691	39.634	19.031	51.90	36.170	21.967	40.385
2	17	19.066	19.453	21.521	24.788	17.275	15.51	34.577	10.513	29.951
3	11	11.337	11.566	12.220	12.852	14.682	6.04	21.025	5.983	14.809
4	5	6.516	6.587	6.505	6.092	11.972	2.91	8.889	3.754	5.492
5	4	3.656	3.642	3.324	2.740	9.487	1.61	2.704	2.507	1.629
6	1	2.014	1.969	1.651	1.191	7.362	0.98	0.602	1.749	0.403
7	2	1.094	1.047	0.804	0.505	5.623	0.64	0.099	1.259	0.085
8	2	1.247	1.131	0.726	0.355	15.994	1.14	0.013	4.196	0.019
Total	120	120	120	120	120	120	120	120	120	120
χ^2	-	1.4445	1.571	2.727	8.057	73.762	16.504	60.052	27.050	21.761
d.f	-	3	3	4	3	7	3	3	4	3
P-value	-	0.6951	0.6660	0.6045	0.0449	< 0.0001	0.0009	< 0.0001	< 0.0001	< 0.0001

Figure 18 shows that the fitted PMFs closely match the observed frequencies of Dataset I, indicating an adequate fit of the competing models.

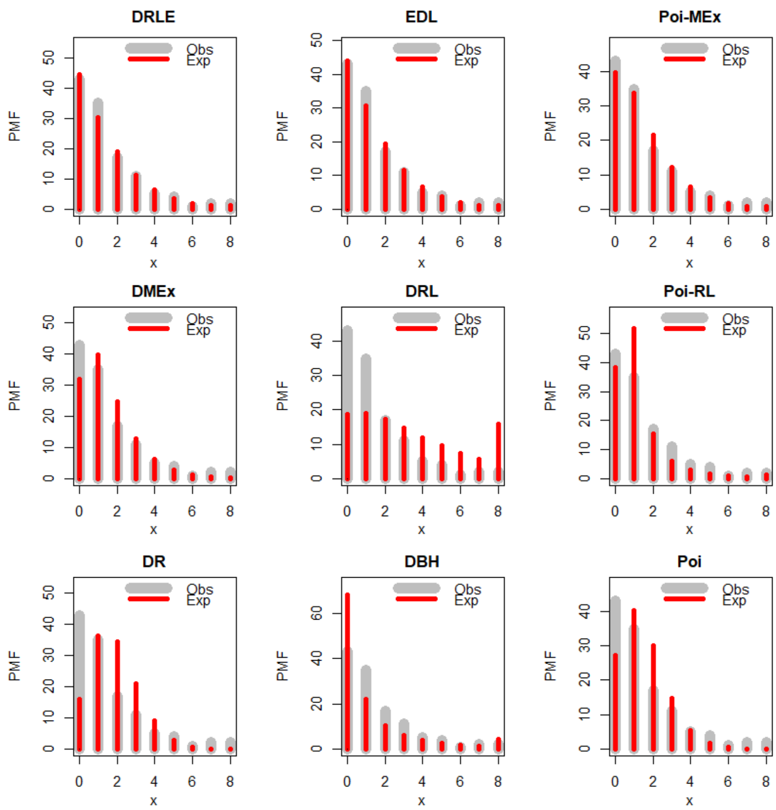

Figure 18. The fitted PMFs for data set I.

6.2. Dataset II: Daily COVID-19 deaths in South Korea

Dataset II consists of daily new COVID-19 death counts reported in South Korea from 15 February to 12 December 2020. The data were obtained from the publicly available source `https://www.`

worldometers.info/coronavirus/country/south-korea/ and exhibit typical characteristics of epidemic count data, including skewness and over-dispersion.

To explore the distributional behavior of the data, nonparametric graphical tools such as boxplots, violin plots, and normal Q–Q plots are employed. These exploratory summaries, shown in Figure 19, provide preliminary insight into dispersion and tail behavior.

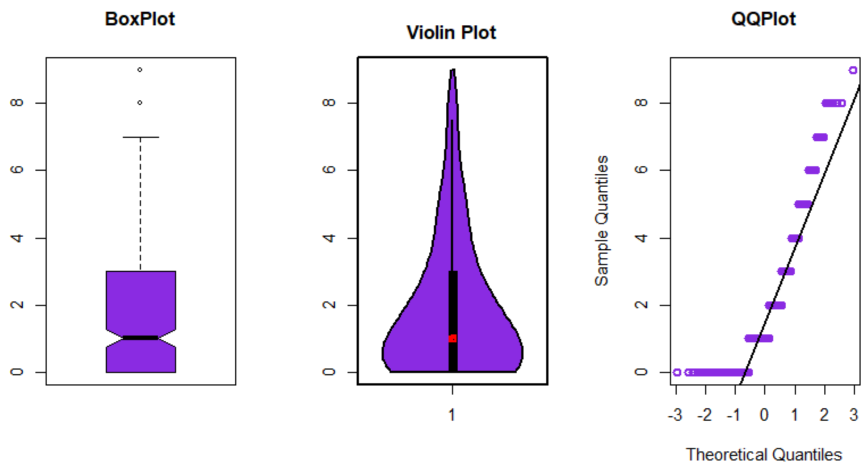

Figure 19. Nonparametric exploratory plots for Dataset II.

Table 19 shows that DRLE achieves the lowest negative log-likelihood and the lowest AIC among all fitted models, indicating a superior likelihood-based fit to Dataset II. Although the parsimonious Poi-MEx model yields a slightly lower BIC, DRLE still performs better for -ℓ, AIC, and goodness-of-fit statistics, indicating that the extra parameter in DRLE indeed provides a meaningful improvement in capturing the data structure rather than merely increasing model complexity. We also observe from Table 20 that the goodness-of-fit tests also confirm the better performance of DRLE, which has the lowest chi-square statistic with the largest p-value among all other models, including Poi-MEx. Together, these results show that DRLE provides the best representation of the data's underlying structure, outperforming all other competing models (including the more parsimonious Poi-MEx) in terms of likelihood-based fit and goodness-of-fit accuracy.

Table 19. Parameter estimates for the fitted models for data II.

Model ↓	$\hat{\alpha}$	$\hat{\beta}$	SE($\hat{\alpha}$)	SE($\hat{\beta}$)	-ℓ	AIC	BIC
DRLE	1.8729	2.9309	0.1786	0.4531	564.807	1133.610	1141.050
EDL	0.5229	0.9304	0.0238	0.1021	564.832	1133.660	1141.100
Poi-MEx	0.9507	-	0.0552	-	566.385	1134.770	1138.490
DMEx	1.2063	-	0.0496	-	576.773	1155.550	1159.260
DRL	2.4574	-	0.1103	-	621.005	1244.010	1247.730
Poi-RL	2.3997	-	0.1193	-	636.588	1275.180	1278.890
DR	0.9029	-	0.0054	-	638.905	1279.810	1283.530
DBH	0.9039	-	0.0203	-	620.466	1242.930	1246.650
Poi	1.9013	-	0.079	-	621.098	1244.200	1247.910

Table 20. Goodness of fit statistics for Dataset II.

X	Observed	DRLE	EDL	Poi-MEx	DMEx	DRL	Poi-RL	DR	DBH	Poi
0	89	90.444	90.336	79.894	61.305	45.125	44.326	29.498	166.600	45.408
1	79	72.811	72.560	77.873	88.745	48.929	44.552	72.405	54.599	86.336
2	49	51.664	51.843	56.927	65.793	45.147	40.809	80.781	26.665	82.047
3	29	34.254	34.438	36.991	40.529	38.425	35.414	61.939	15.541	52.014
4	19	21.767	21.870	22.535	22.845	31.152	29.662	35.682	10.015	24.725
5	17	13.435	13.470	13.179	12.222	24.447	24.229	15.985	6.886	9.402
6	9	8.118	8.114	7.493	6.317	18.743	19.427	5.664	4.953	2.979
7	6	4.827	4.805	4.174	3.186	14.121	15.353	1.603	3.682	0.809
8	6	2.834	2.807	2.288	1.578	10.495	11.995	0.364	2.808	0.192
9	1	3.845	3.757	2.647	1.479	27.415	38.232	0.078	12.251	0.061
Total	304	304	304	304	304	304	304	304	304	304
χ^2	-	3.080	3.238	7.513	32.115	107.899	131.003	184.993	109.335	115.896
d.f	-	5	5	6	6	8	8	5	6	4
P-value	-	0.6877	0.6633	0.2760	< 0.0001	< 0.0001	< 0.0001	< 0.0001	< 0.0001	< 0.0001

Figure 20 graphically supports these findings by displaying the fitted probability mass functions (PMFs) for the models against the observed data. The DRLE and EDL models closely trace the observed frequencies across all values of X, highlighting their ability to capture the underlying distribution effectively. Models such as DR, DBH, and Poi deviate markedly, especially in the tails of the distribution, demonstrating overdispersion or underdispersion issues.

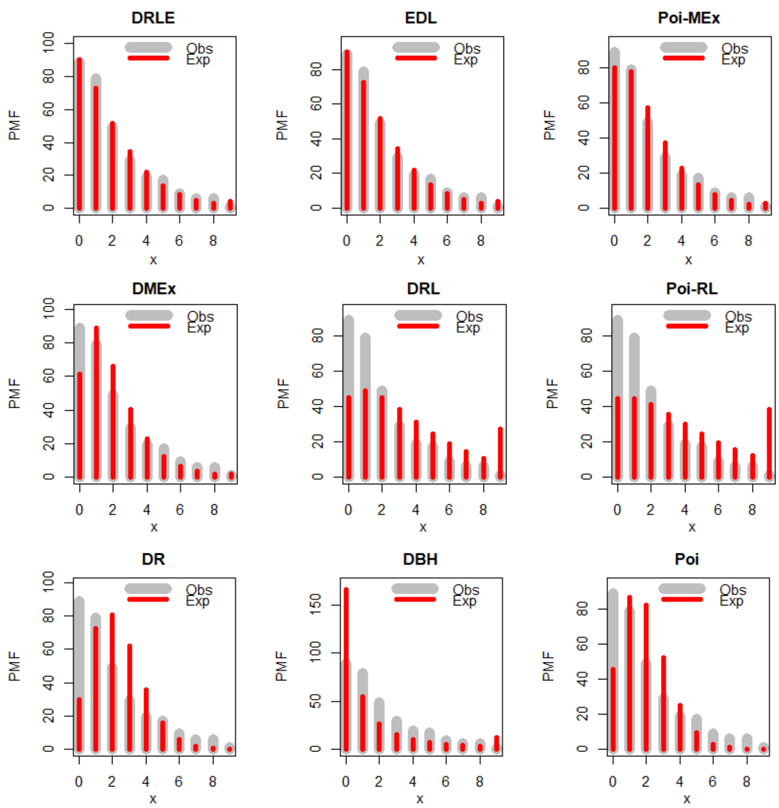

Figure 20. The fitted PMFs for data set II.

7. Conclusions

In this paper, we proposed the discrete Ramos–Louzada exponential (DRLE) distribution as a new two-parameter discrete model obtained by discretizing the survival function of the continuous Ramos–Louzada exponential distribution. The proposed model possesses closed-form expressions for its probability mass function, cumulative distribution function, survival function, hazard rate, moment generating function, and several important distributional characteristics. Furthermore, theoretical results established log-concavity, unimodality, and a strictly increasing discrete hazard rate, providing a mathematically tractable framework for modeling count data arising in reliability and lifetime studies.

The flexibility of the proposed distribution was investigated through analytical, numerical, and graphical analyses. Numerical illustrations demonstrated that the model can accommodate different levels of dispersion, skewness, tail behavior, and hazard-rate patterns through appropriate choices of the model parameters. The real-data applications involving biological and COVID-19 datasets further illustrated that the DRLE distribution provides a competitive fit relative to several discrete lifetime distributions according to likelihood-based criteria and goodness-of-fit statistics. Moreover, maximum likelihood and Bayesian estimation procedures were developed for the proposed model. The simulation study examined their finite-sample behavior under two representative parameter settings and several sample sizes. The numerical results indicated that Bayesian estimation produces stable posterior summaries and satisfactory interval estimates across the considered scenarios, supported by effective sample sizes, Monte Carlo standard errors, acceptance rates, and Gelman–Rubin convergence diagnostics. For the maximum likelihood approach, the simulation results also revealed that estimation accuracy depends on the underlying parameter configuration. In particular, the second simulation scenario exhibits relatively large estimation errors despite successful numerical convergence, indicating that numerical convergence alone should not be interpreted as evidence of attainment of the global optimum. Accordingly, the conclusions drawn from the simulation study have been intentionally restricted to the scenarios investigated in this paper.

Despite its favorable analytical properties, the proposed model has several limitations. First, for the simulation study, we considered only two representative parameter settings and therefore do not exhaustively cover the full parameter space of the DRLE distribution. Second, parameter estimation relies on numerical optimization for maximum likelihood estimation and Markov chain Monte Carlo sampling for Bayesian inference, both of which may become computationally demanding for large datasets or challenging parameter configurations. Finally, we focus on independent observations obtained through the floor discretization of the continuous baseline model.

Future research directions

Several promising research directions remain open:

- **Expanded simulation studies:** Future simulation experiments should investigate a wider range of parameter configurations, including values close to the parameter boundary, weakly identifiable settings, under-dispersed and highly over-dispersed cases, and different tail regimes. Additional numerical studies based on multiple optimization starting values, likelihood-profile analyses, computational cost comparisons, and Bayesian prior sensitivity analyses would provide a more comprehensive assessment of estimator performance.

- **Regression models:** Extending the DRLE distribution to generalized count regression models by incorporating covariate effects through suitable link functions.
- **Alternative Bayesian procedures:** Investigating alternative prior specifications, adaptive MCMC algorithms, Hamiltonian Monte Carlo methods, and approximate Bayesian inference techniques to improve computational efficiency.
- **Model extensions:** Constructing generalized, zero-inflated, hurdle, multivariate, or dependent versions of the DRLE distribution to increase modeling flexibility.
- **Incomplete and censored data:** Developing estimation procedures for censored, truncated, interval-censored, or missing count data commonly encountered in reliability and survival analysis.
- **Alternative estimation methods:** Comparing maximum likelihood and Bayesian inference with composite likelihood, generalized method of moments, estimating equations, robust estimation procedures, and minimum-distance estimation methods.
- **Reliability and maintenance applications:** We consider independent count observations. Extending the DRLE distribution to multicomponent reliability systems, dependent competing-risk models, repairable systems, and preventive maintenance optimization constitutes an interesting direction for future research.

Overall, the DRLE distribution provides a mathematically tractable and flexible addition to the family of discrete lifetime and count distributions. Although further theoretical and computational investigations are warranted, the analytical properties, estimation procedures, and empirical applications presented in this study suggest that the proposed model constitutes a useful alternative for modeling discrete lifetime and count data encountered in biology, epidemiology, reliability, and related application areas.

Data availability statement

The data that supports the findings of this study are available within the article. The data supporting the findings of this study are presented within the article.

Author contributions

Ahood Abdalrahman Alazwari: Writing-original draft, Validation, Methodology, Formal analysis, Conceptualization, Writing-review, Investigation. **Ayse Metin Karakas:** Writing-original draft, Validation, Methodology, Formal analysis, Conceptualization, Writing-review, Investigation. **Fatma Bulut:** Writing-original draft, Validation, Methodology, Formal analysis, Conceptualization, Writing-review, Investigation. **Eslam Hussam:** Writing-original draft, Validation, Methodology, Formal analysis, Conceptualization, Writing-review, Investigation. **Muhammad Ahsan-ul-Haq:** Writing-original draft, Validation, Methodology, Formal analysis, Conceptualization, Writing-review, Investigation. **Samirah Alzubaidi:** Writing-original draft, Validation, Methodology, Formal analysis, Conceptualization, Writing-review, Investigation. **Amani Alrumayh:** Writing-original draft, Validation, Methodology, Formal analysis, Conceptualization, Writing-review, Investigation. **M. E. Sobh:** Writing-original draft, Validation, Methodology, Formal analysis, Conceptualization, Writing-review, Investigation. All authors have read and approved the final version of the manuscript for publication.

Use of Generative-AI tools declaration

The authors declare that no generative artificial intelligence (AI) tools were used in the preparation of this manuscript.

Acknowledgments

The authors extend their appreciation to Umm Al-Qura University, Saudi Arabia for funding this research work through grant number: 26UQU4340101GSSR03.

Funding

This research work was funded by Umm Al-Qura University, Saudi Arabia under grant number: 26UQU4340101GSSR03.

Conflict of interest

The authors declare no conflicts of interest.

References

1. A. Z. Afify, M. Ahsan-ul-Haq, H. M. Aljohani, A. S. Alghamdi, A. Babar, H. W. Gómez, A new one-parameter discrete exponential distribution: properties, inference, and applications to COVID-19 data, *J. King Saud Univ.-Sci.*, **34** (2022), 102199. http://dx.doi.org/10.1016/j.jksus.2022.102199
2. M. Ahsan-ul-Haq, On Poisson moment exponential distribution with applications, *Ann. Data Sci.*, **11** (2024), 137–158. http://dx.doi.org/10.1007/s40745-022-00400-0
3. K. Al-Harbi, A. Fayomi, H. Baaqeel, A. Alsuraihi, A novel discrete linear-exponential distribution for modeling physical and medical data, *Symmetry*, **16** (2024), 1123. http://dx.doi.org/10.3390/sym16091123
4. H. M. Aljohani, F. M. Zaghdoun, M. A. Meraou, A. S. Alharthi, W. A. J. Almohri, Z. I. Kalantan, et al., A novel extension of the exponential distribution with application in modeling complex lifetime and environmental data, *Sci. Rep.*, **15** (2025), 33581. http://dx.doi.org/10.1038/s41598-025-18711-6
5. I. Alkhairy, Classical and Bayesian inference for the discrete Poisson Ramos-Louzada distribution with application to COVID-19 data, *Math. Biosci. Eng.*, **20** (2023), 14061–14080. http://dx.doi.org/10.3934/mbe.2023628
6. A. Balubaid, H. Klakattawi, D. Alsulami, On the discretization of the Weibull-G family of distributions: properties, parameter estimates, and applications of a new discrete distribution, *Symmetry*, **16** (2024), 1519. http://dx.doi.org/10.3390/sym16111519

7. J. M. Bernardo, A. F. M. Smith, *Bayesian theory*, John Wiley and Sons, 2000.
8. W. Bodhisuwan, S. Sangpoom, The discrete weighted Lindley distribution, *2016 12th International Conference on Mathematics, Statistics, and Their Applications (ICMSA)*, IEEE, 2016, 99–103. http://dx.doi.org/10.1109/ICMSA.2016.7954317
9. B. P. Carlin, T. A. Louis, Bayes and empirical Bayes methods for data analysis, *Stat. Comput.*, **7** (1997), 153–154. http://dx.doi.org/10.1023/A:1018577817064
10. A. S. Eldeeb, M. Ahsan-ul-Haq, M. S. Eliwa, A discrete Ramos–Louzada distribution for asymmetric and over-dispersed data with leptokurtic-shaped: properties and various estimation techniques with inference, *AIMS Math.*, **7** (2022), 1726–1741. http://dx.doi.org/10.3934/math.2022099
11. M. El-Morshedy, M. S. Eliwa, H. Nagy, A new two-parameter exponentiated discrete Lindley distribution: properties, estimation and applications, *J. Appl. Stat.*, **47** (2020), 354–375. http://dx.doi.org/10.1080/02664763.2019.1638893
12. M. El-Morshedy, M. S. Eliwa, E. Altun, Discrete Burr-Hatke distribution with properties, estimation methods and regression model, *IEEE Access,* **8** (2020), 74359–74370. http://dx.doi.org/10.1109/ACCESS.2020.2988431
13. J. K. Ghosh, R. V. Ramamoorthi, *Bayesian nonparametrics*, Springer, 2003. http://dx.doi.org/10.1007/b97842
14. A. M. Karakaş, F. Bulut, The new Gompertz distribution model and applications, *Symmetry*, **17** (2025), 843. http://dx.doi.org/10.3390/sym17060843
15. A. M. Karakaş, F. Bulut, The half-logistic generalized power Lindley distribution: theory and applications, *Symmetry*, **17** (2025), 1936. http://dx.doi.org/10.3390/sym17111936
16. T. Nakagawa, S. Osaki, The discrete Weibull distribution, *IEEE Trans. Reliab.*, **24** (1975), 300–301. http://dx.doi.org/10.1109/TR.1975.5214915 .
17. S. D. Poisson, *Recherches sur la probabilité des jugements en matière criminelle et en matière civile: précédées des règles générales du calcul des probabilités*, Bachelier, Paris, 1837.
18. C. P. Robert, G. Casella, *Monte Carlo statistical methods*, 2 Eds., Springer, 2004. http://dx.doi.org/10.1007/978-1-4757-4145-2
19. D. Roy, Discrete Rayleigh distribution, *IEEE Trans. Reliab.*, **53** (2004), 255–260. http://dx.doi.org/10.1109/TR.2004.829161